TRIBHUVAN UNIVERSITY

INSTITUTE OF ENGINEERING

PULCHOWK CAMPUS

THESIS NO: M-108—MSMDE-2024-2026

DYNAMIC BEHAVIOR ANALYSIS OF BEAM SUPPORTED BY SPRINGS WITH LUMPED MASS AT THE CENTRE

BY

SAURAB KUMAR YADAV

A THESIS REPORT SUBMITTED TO THE DEPARTMENT OF MECHANICAL AND AEROSPACE ENGINEERING IN PARTIAL FULFULLMENT OF THE REQUIREMENTS FOR THE DEGREE OF MASTERS OF SCIENCE IN MECHANICAL SYSTEMS DESIGN AND ENGINEERING

DEPARTMENT OF MECHANICAL AND AEROSPACE ENGINEERING

LALITPUR, NEPAL

APRIL 2026

COPYRIGHT

TRIBHUVAN UNIVERSITY

INSTITUTE OF ENGINEERING

PULCHOWK CAMPUS

DEPARTMENT OF MECHANICAL AND AEROSPACE ENGINEERING

The undersigned certify that they have read, and recommended to the Institute of Engineering for acceptance a thesis entitled **"Dynamic Behaviour Analysis of Beam Supported by Springs with Lumped Mass at the Centre"** submitted by **Saurab Kumar Yadav** (080MSMDE021) in the partial fulfillment of the requirements for the degree of Master of Science in Mechanical System Design and Engineering.

.....

Supervisor: Dr. Laxman Poudel

Professor

Department of Mechanical and Aerospace Engineering

Pulchowk Campus

.....

Supervisor: Dr. Sudip Bhattarai

Assistant Professor

Department of Mechanical and Aerospace Engineering

Pulchowk Campus

.....

External examiner: Er. Pradhumna Adhikari

U.S. Embassy

.....

Committee Chairperson:

Head of the Department

Department of Mechanical and Aerospace Engineering

Pulchowk Campus

Tribhuvan University
Institute of Engineering
Department of Mechanical and Aerospace Engineering
Pulchowk Campus

Date: April 24 2026

ABSTRACT

This study investigates the dynamic behavior of beams supported by elastic springs at both ends and carrying a lumped mass at the centre, a configuration commonly found in practical mechanical and structural systems where support flexibility and attached components influence vibration response. The governing equations for both longitudinal and transverse free vibration were derived using Hamilton's principle based on Euler–Bernoulli beam theory, and analytical solutions were developed for symmetric and asymmetric spring-supported cases with and without a central lumped mass. Numerical modal analysis was then performed in ANSYS Workbench to validate the analytical model. The results showed that longitudinal natural frequencies were significantly higher than transverse frequencies due to greater axial stiffness, while the introduction of the central lumped mass reduced natural frequencies in a strongly mode-dependent manner. Modes with significant midpoint displacement experienced substantial frequency reduction, whereas modes having a nodal region near the centre remained nearly unaffected. Support asymmetry further shifted modal frequencies, nodal locations, and deformation patterns, producing unsymmetrical mode shapes. The close agreement between analytical and ANSYS results confirmed the validity of the developed formulation. Overall, the study demonstrates that support flexibility, mass concentration, and modal participation play decisive roles in governing the vibration characteristics of beam–spring–mass systems.

ACKNOWLEDGEMENTS

I would like to express my sincere gratitude to Prof. Dr. Laxman Poudel, Dr. Sudip Bhattarai and Prof. Mahesh Chandra Luintel for their valuable guidance, encouragement and support throughout the completion of my thesis. Their insightful suggestions and academic expertise have greatly contributed in shaping this research work. I am grateful for their time and effort in supervising my work which helped a lot in refining this work. Their mentorship and guidance have contributed highly in my overall academic development.

I would also like to thank Aastha Bajracharya for her continuous motivation and support throughout the completion of my thesis. Her encouragement and assistance were highly valuable during this research work.

TABLE OF CONTENTS

LIST OF FIGURES

LIST OF TABLES

LIST OF ABBREVIATIONS

ANSYS	Analysis System (Finite Element Analysis Software)
FEM	Finite Element Method
PDE	Partial Differential Equation

LIST OF SYMBOLS

A	Cross-sectional Area of Beam
Ad	Cross-sectional Area of Disc
c	Axial Wave Velocity
E	Young's Modulus
EA	Axial Rigidity of Beam
EI	Flexural Rigidity of Beam
Hz	Hertz (Frequency Unit)
I	Second Moment of Area
kLH	Left Horizontal Spring Stiffness
kLV	Left Vertical Spring Stiffness
kRH	Right Horizontal Spring Stiffness
kRV	Right Vertical Spring Stiffness
L	Length of Beam
m	Meter
Md	Lumped Disc Mass at Beam Centre
N	Newton
Pa	Pascal
td	Thickness of Disc
μ	Mass Ratio Parameter
ρ	Material Density
ρA	Mass per Unit Length

CHAPTER 1. INTRODUCTION

1.1 Background

The structural element of a beam and rods is a vital constituent of engineering systems such as bridges, mechanical shafts, or frame structures. The vibration properties of these members are essential for stability analysis and proper operation of a particular system. Hence, the analysis of vibrations plays a central role in the field of structural dynamics. Conventional approaches, especially Euler-Bernoulli theory, have been applied extensively for the calculation of natural frequencies and mode shapes for various types of boundary conditions (Chen, 1963; Laura et al., 1987). Nonetheless, in actual engineering applications, there exist few cases where supports of structural members are perfectly rigid. Elasticity is often present as a result of foundation, joints, or connection flexibility, which makes it difficult to neglect. Elastically restrained supports can easily be simulated using springs, resulting in a drastic change in stiffness and boundary conditions. Many researchers, such as Goel (1976) and Liu et al. (1988), have shown the significance of the elasticity of the supports for the vibration behavior. Xiao et al. (2013) and Hozhabrossadati et al. (2015) have carried out research in this field in a more general approach towards elastically restrained beams with a variety of attachments.

In addition to the role of boundary flexibility, another important aspect that affects the dynamic behavior is the inclusion of concentrated or lumped masses at certain sections of the beam. In actual practice, there may be cases where some mechanical devices such as discs, sensors, and actuators could be added to the structural element. Initial research into this concept was carried out by Chen (1963), while subsequent work by Laura et al. (1987) and Liu and Yeh (1987) revealed that a single lumped mass could play a significant role in the system's natural frequency and vibration modes. Combining the effect of elastic supports and lumped masses leads to increased complexity since both mass and stiffness distributions act together. Some examples of related studies include the study by Kukla (1994), which focused on axially loaded beams with lumped masses and elastic support conditions, and the work done by Banerjee (2012) using the dynamic stiffness method for spring-mass systems on beams. However, few investigations have been done on the dynamics of the beam supported by spring at both ends and having a concentrated mass in its centre simultaneously under both axial and lateral vibration effects, hence the significance of the current study.

1.2 Statement of problem

Though many works have been carried out on vibration analysis of beams, existing studies mainly concentrate on the analysis of structures with only spring boundary support or lumped masses but not both at once. In practical engineering problems, such combination may occur, which has not been analyzed enough in existing literature. The interaction of spring supported boundary conditions and lumped masses placed symmetrically relative to the midpoint has not been investigated well yet.

As far as practical applications go, beams are often mounted on elastic supports as well as having other elements attached to them at different points, such as disc or other machine parts. This adds inertia, while elasticity of supports adds complexity to boundary stiffness. This complicates matters to the point where no simplifications can be applied in order to make predictions. There is a need for a thorough analytical approach in this case.

This research work seeks to fill this gap by considering the dynamical behavior of a beam having elastic supports at both ends and having a lumped mass at its midsection. Equations of motion are established based on Hamilton's principle for an energy-based formulation. Exact solutions are found for longitudinal and transverse vibration problems, and the findings are validated using computer-based simulation software ANSYS. This comprehensive study reveals more about the effect of boundary conditions and concentrated masses on the dynamical behavior of beams, which plays a vital role in the development of engineering systems.

1.3 Objectives of research

The objective of this research is to analyze the dynamic behavior of beams supported by springs at both ends with a lumped mass located at the centre through analytical modelling and numerical simulation.

1.3.1 Main objective

- To investigate the dynamic behavior of beams supported by springs at both ends with a lumped mass at the centre using analytical and numerical approaches.

1.3.2 Specific objectives

- To derive the governing equations of motion for beams supported by springs using Hamilton's principle.

- To develop analytical solutions for the longitudinal and transverse vibration response of beams supported by springs with and without a lumped mass at the centre..
- To simulate the dynamic response of the beam system using ANSYS software.
- To compare the analytical solutions with the numerical results obtained from ANSYS simulations.

1.4 Rationale of the study

The need for understanding the vibration characteristics of beam structures in modern engineering applications has led to the design of this experiment. There exist various beam structures supported by elastic means like spring supports, where there is a need to consider the flexibility of the boundaries while conducting the analysis of the system dynamics. Further, there are systems with attached masses, like discs or sensors on particular sections of the beam.

Despite extensive investigations in beam vibration analysis, most of them considered either the elastic boundary or the point mass alone. The combined effect of spring support at the boundary and presence of a point mass located at the centre has not received much attention even though it is an important issue from practical considerations. Such an approach results in complicated dynamics, causing changes in natural frequencies and mode shapes along with symmetric and antisymmetric oscillations.

Thus, the objective of this work is to formulate a comprehensive model to examine the behavior of a beam resting on two springs located at each end, having a lumped mass at its midpoint. The formulation of equations of motion is done based on Hamilton's principle to maintain energy considerations, and the solutions are found analytically for longitudinal and transverse vibrations. Moreover, verification of results is done through finite element software ANSYS, thereby confirming the accuracy of the analytical solutions. This approach offers significant insights regarding the effect of boundary flexibility and the presence of a mass, which can be utilized for practical applications in structural engineering designs.

1.5 Limitations of research

- The beam is assumed to follow Euler–Bernoulli beam theory, which neglects shear deformation and rotary inertia effects.

- The analysis focuses only on free vibration and does not consider damping or external forcing effects.
- The lumped mass is assumed to be located exactly at the centre of the beam, and material properties are considered uniform throughout the beam.

CHAPTER 2. LITERATURE REVIEW

The fundamental analytical basis of analyzing a beam/rod loaded with an attached mass was provided by Chen (1963). The primary finding from the work included the fact that a concentrated mass could not be considered simply as an add-on effect as the same produces an inertia discontinuity which affects the natural frequencies and mode shapes of the member. This aspect holds tremendous significance for the current research work, wherein the beam is also subjected to an additional concentrated mass at its mid-section. It was evident from their work that the attached mass needs to be considered while solving for the vibration problem in the continuous beam. In fact, the early theoretical basis of considering a central mass as a governing dynamic aspect.

Goel (1976) studied free vibration analysis of a beam-mass model whose ends were elastically supported and gave one of the earliest examples of the coupled treatment of both support flexibility and mass attachment. The most significant contribution of this research is the conclusion that elastic supports greatly influence the frequencies and that the combination of restraint elasticity and mass attachment gives rise to a behavior much more complicated than each individual factor. This study clearly shows that practical support characteristics should be taken into consideration when the vibrations of the model are to be determined correctly.

Laura et al. (1987) expanded the analysis of concentrated mass to include beams and plates having concentrated masses and considering the significance of mass magnitude and its position. Their main contribution was proving that the placement of the concentrated mass has a critical impact on the lower vibration modes and frequency shift due to the presence of such concentrated mass. This has increased the importance of concentrated-mass beams because vibration behavior is dependent not only on the size but also on the position of the concentrated mass.

In another development to the area, Liu et al. (1988) investigated beams with edge conditions elastically restrained and having concentrated masses at some locations between the two supports. The key contribution of their work was the confirmation that the combined effects of flexible boundary conditions and internal loads significantly affect the frequency distribution and the associated mode shapes. The paper also revealed that the presence of internal masses causes localized behavior while the edge

conditions cause global effects. The findings support the need for joint analysis of the central mass and end springs.

Kukla (1994) studied the free vibrations of axially loaded beams with concentrated masses and elastic supports. The main contribution from this paper is proving that axial loading, concentrated masses, and elastic supports all have a coupling effect on the dynamic behavior of the beam. This research extended previous works which only included flexural behavior of beams to include the effects of axial loading, thereby proving that concentrated masses were still relevant in such cases.

A new dynamic stiffness method for beam-spring mass structures has been proposed by Banerjee (2012). They have made an important contribution to the research area through their more efficient computational model. The main achievement of this work has been that it has been shown how a dynamic system incorporating beam and spring-mass sub-system can be solved effectively without any oversimplification.

Xiao et al. (2013) developed a more general approach to analyze elastically restrained beams subjected to arbitrary attachments of various kinds. The main contribution of their study was in presenting a generalized analysis of the beam-attachment system, wherein the modal characteristics of the beam are governed by the combined effects of its boundary conditions, attachment type, and attachment distribution. In contrast to previous research which has concentrated on particular cases, Xiao et al. emphasize the importance of developing general approaches for solving the problem. This underlines the relevance of the analytical approach to non-classical beams.

Hozhabrossadati et al. (2015) investigated a beam with elastic boundary supports at the ends and a spring-rotational mass system in the middle span of the beam. The most important result from their research is that an introduced dynamic sub-system in the middle of the beam can greatly affect the natural frequencies and mode shapes, particularly those of the lower modes. While Hozhabrossadati's intermediate dynamic system incorporates the effect of rotational movement, the critical point stays the same, and that is, the mid-span attachment becomes the key element of the beam.

According to Abbas et al., (2016), an application of a transfer matrix approach was used in the free vibration study of beams having point masses supported by elastic supports. One of the key findings in their investigation is the finding that discrete attachments in beams can be represented as local dynamic systems without losing any systematic study

of the entire system. It turns out that the locally attached masses have the ability to affect significantly the global vibration response of the beam structure depending on the coupling of attachment with the beam structure.

The research by Kumar et al. (2019) dealt with free vibrations of spring-mounted beams and stressed the significance of non-classical boundary conditions. The most important result of the analysis conducted by Kumar et al. (2019) was the explicit recognition of the stiffness of the beam supports as a crucial factor defining the natural frequencies of the beam. It is especially significant to your work because the beam you are investigating is also fixed with springs at its ends. Although the paper does not have the specific case of lumped mass in the middle, it provides ample justification for the boundary condition aspect of your work.

The main achievement reported by Lee et al. (2023) in their recent research is the affirmation that the interaction among the elastic restraint, concentrated mass, and axial force still represents a topic worth researching today. In spite of the fact that the beam considered by the authors is tapered, unlike the uniform one, the importance of the finding cannot be overlooked; rda the flexible nature of boundary conditions and concentrated masses attached at certain locations still define the modal characteristics of beam systems.

Yayli et al. (2024) have investigated a beam supported by an elastic foundation and having its end supported by an elastic constraint and presented a relatively efficient analytical solution for vibration of such a beam. The key point made in this paper is the observation that even without any applied concentrated load, the conditions of elastic restraints can greatly change the frequency equation and dynamic behavior of a beam. The paper is especially interesting because of the important contribution it makes to the theory of flexible boundary condition modelling, which represents one of the most crucial elements in the present thesis.

CHAPTER 3. METHODOLOGY

3.1 Conceptual Framework

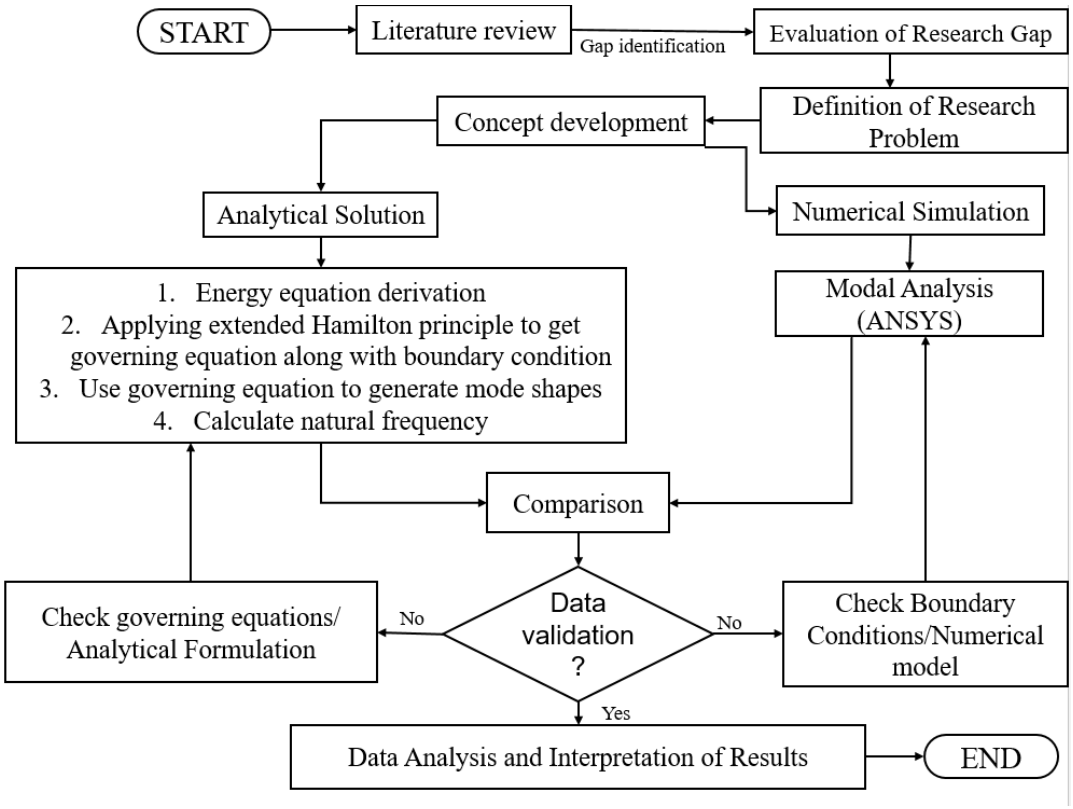

Figure 1. Schematic diagram of research process

In the present research work, the methods used for the analysis include both analytical and numerical approaches that investigate the dynamic behavior of the beam supported by elastic supports at both ends, while there is a mass concentration at its centre. The objective of the current research is to find out the natural frequency, mode shapes, and influence of stiffness of the supports and concentrated mass on the dynamics of the structure. For the investigation of the present topic, two lines of investigation were followed: analytical vibrations and numerical ANSYS approach.

First, the literature review was conducted to identify the research problem and develop the mathematical model. After that, the governing equation was developed based on Hamilton's principle and Euler-Bernoulli beam theory for both longitudinal and transverse vibrations. Simultaneously, the formulation of the FEM was carried out using ANSYS software with equivalent dimensions and material properties and spring boundary

conditions. These results were compared to ensure validation. Further, any discrepancy identified was again verified. After validating the results, interpretation was done.

3.2 Literature Review

The project began with a detailed literature review regarding vibration of beams having elastic supports, vibration of beams having masses attached to them, and techniques adopted for mode analysis. Literature about vibrations of beams supported by springs, vibrations of beams with masses attached to them, and continuous vibration system analysis has been critically reviewed. Concepts of vibration, classical analysis, and eigenvalue analysis have also been explored.

This is where it has been found that most researchers have concentrated on rigidly supported beams or simply un-loaded beams. It can be seen that few researchers have taken up the challenge to conduct studies regarding the effects of spring supports in the two extreme ends of the beams along with loading the centre of the beam with a lumped mass.

3.3 Gap Identification

From a survey of literature, it is evident that minimal consideration has been given to the impact of both flexible supports and centrally concentrated mass on the dynamics of the beam. The previous studies only analyzed the effects of either fixed or simply supported beams. However, in reality, flexible supports are always considered. Moreover, the presence of concentrated mass in the mid-span region of the beam significantly influences the dynamic behavior of the beam.

Yet another gap identified during the literature review is that the study has not yet compared the solution obtained in analytical form with the solution obtained using finite element modal analysis. In order to fill this gap, the present study deals with the problem of beam on spring with concentrated mass at the centre.

3.4 Evaluation of Research Gap

After identifying the problem, the significance and feasibility of the problem were assessed. The mathematical model of beam-spring-mass system can be utilized for modeling some engineering problems such as a flexible shaft, a pipeline transporting some devices, bridge element carrying suspended devices, and mechanical elements with elastic boundary conditions. Hence, it is necessary to analyze the vibration characteristics of the beam-spring-mass model.

Academic value of this research can also be found in the sense that it will make theoretical contribution in the field of classical vibrations of beams by means of using elastic boundary conditions and masses. Therefore, the selected research problem can be considered to be technically sound and feasible.

3.5 Definition of Research Problem

The problem statement was to determine the dynamic behavior of a uniform beam supported by springs at both ends under a point load applied to the centre of the beam. The objectives included formulating the differential equations of motion, natural frequencies, and vibration modes for both longitudinal and transverse vibrations.

This special attention was given to studying the correlation between spring stiffness and mass change in terms of beam modes. Furthermore, the problem was widened to compare the theoretical results with numerical calculations using ANSYS.

3.6 Concept Development

The problem was clearly formulated, followed by conceptual modeling of the beam system. It was assumed that the beam was homogenous, linearly elastic, and had uniform sections. Spring systems were introduced at the two ends, representing flexible supports, whereas a point load was applied at mid-span

Considerations were made of two types of vibrations; the first type of vibrations considered is longitudinal vibrations, which depend on axial deformation, while the second type is transverse vibrations, which depend on bending deformation.

3.7 Analytical Solution

At the analytical stage, the mathematical model of the beam-spring-mass system was developed. Kinetic and potential energy of the beam, springs, and lumped masses were calculated. Based on the Hamiltonian principle, the differential equation governing the system and its boundary/compatibility equations were developed.

This resulted in solving an eigenvalue problem, where characteristic equations, natural frequencies, and mode shapes were derived. Various mathematical techniques were adopted for the longitudinal and transverse vibrations analysis. The first three natural frequencies and the corresponding normalized mode shapes were chosen for subsequent studies.

3.8 Numerical Simulation

The numerical analysis for the problem is carried out by using ANSYS Workbench. A model of the beam was created using the beam element. The material properties of the beam, dimensions, and spring supports were input based on data from the analytical model. Point mass is attached to the beam using the point mass element.

The modal analysis was conducted in order to obtain the first three natural frequencies and their modes. Particular emphasis was placed on ensuring that there were no discrepancies between the analytical and numerical boundary conditions.

3.9 Comparison

The comparison was carried out between the analytical and numerical methods based on natural frequency and corresponding mode shapes. The percentage error approach was used to calculate the error between two methods. Mode shapes were also analyzed visually to check whether the analytical mode shapes match ANSYS mode shapes or not.

Good correlation between the two methods confirms the reliability of the derived governing equations and validates the numerical model.

3.10 Data Validation

The results were validated using the process of iterations. In case the error between the analytical frequency and the frequency obtained using ANSYS software became higher than the tolerance limit, the governing equations, spring constants, meshing, and boundary conditions were reconsidered. The required changes were incorporated to obtain consistent results.

This process ensured that both models accurately represented the physical beam–spring–mass system.

3.11 Data Analysis and Interpretation of Results

With validation in place, the data collected were analyzed to determine the influence of the stiffness of the support and the central mass on the dynamic response of the system. The observations made included that with the increase in the stiffness of the spring, the natural frequency of the system increases.

Symmetric and antisymmetric motion characteristics were identified in the vibration modes. These findings may prove useful in future studies on vibration control and spring beam designs.

CHAPTER 4. DESIGN & MODELLING

4.1 Beam-Spring-Mass System

In terms of methodology of the study, the first stage is to provide information about the geometry of the beam-spring-mass system. Specifically, the homogenous beam is considered during this research. At the same time, the beam is attached to the two boundary points by means of the linear elastic springs. Flexible boundary conditions are selected instead of the stiff rigid boundary conditions which can be found in real engineering problems. For the purpose of modeling additional masses of the beam, a mass point is considered located at the middle of the beam. The analysis of the beam is made under the framework of the Euler-Bernoulli beam theory when the shearing effects and rotary inertia are not considered. In other words, all physical parameters of the beam (beam length, Young's modulus, density, cross-sectional area, and moment of inertia) are known. The spring constants at each boundary are also provided. Finally, the information about mass point's weight is known.

4.2 Governing Equations (Hamilton's Principle)

Once the geometry of the beam is established, the equation of motion will be derived using Hamilton's principle. The use of Hamilton's principle is typical in vibrational analysis because this principle provides an elegant method for the derivation of the equations of motion through energy considerations. According to Hamilton's principle, the dynamic response of any system can be found by minimizing the variation of the integral of the difference between kinetic energy and potential energy. In this study, the kinetic energies of the beam and the lumped masses will be considered first. After that, the strain energy of the beam due to deformation and the potential energy associated with the spring supports are considered. All of these energies are then substituted into Hamilton's principle to derive the differential equations of motion.

I. Longitudinal vibration without lumped mass

The governing partial differential equation is

$$\rho A \frac{\partial^2 u}{\partial t^2} = \frac{\partial}{\partial x}\left(EA \frac{\partial u}{\partial x}\right).$$

Since E and A are constant,

$$\rho A \frac{\partial^2 u}{\partial t^2} = EA \frac{\partial^2 u}{\partial x^2}.$$

The spring-supported boundary conditions are

$$EAU'(0) - k_{LH}U(0) = 0$$

and

$$EAU'(L) + k_{RH}U(L) = 0$$

II. Longitudinal vibration with lumped mass

For a uniform rod with a concentrated disc mass at $x = a$, the governing equation can be written in delta-function form as

$$[\rho A + M_d\,\delta(x-a)]\,\ddot{u}(x,t) - EA\,u_{xx}(x,t) = 0.$$

The spring-supported boundary conditions are

$$EAU'(0) - k_L U(0) = 0,$$

$$EAU'^{(L)} + k_R U(L) = 0.$$

III. Transverse vibration without lumped mass

The governing transverse bending PDE is

$$\rho A\,\ddot{w}(x,t) + EI\,w_{xxxx}(x,t) = 0.$$

The four boundary conditions used in the supplied PDF are as follows.

At $x = 0$

Boundary condition 1: zero bending moment

$$EI\,w_{xx}(0,t) = 0.$$

Boundary condition 2: shear-spring relation

$$EI\,w_{xxx}(0,t) + k_{LV}\,w(0,t) = 0.$$

At $x = L$

Boundary condition 3: zero bending moment

$$EI\,w_{xx}(L,t) = 0.$$

Boundary condition 4: shear-spring relation

$$EI\,w_{xxx}(L,t) - k_{RV}\,w(L,t) = 0.$$

IV. Transverse vibration with lumped mass

The governing transverse bending PDE is

$$\rho A\, w_{tt}(x,t) + EI\, w_{xxxx}(x,t) + m_d\, \delta\left(x - \frac{L}{2}\right) w_{tt}(z,t) = 0.$$

The end boundary conditions are

$$EI\, w_{xx}(0,t) = 0,$$

$$EI\, w_{xxx}(0,t) + k_{LV}\, w(0,t) = 0,$$

$$EI\, w_{xx}(L,t) = 0,$$

$$EI\, w_{xxx}(L,t) + k_{RV}\, w(L,t) = 0$$

4.3 Analytical Solution-Longitudinal Vibration (No Lumped Mass)

Following the derivation of the equations, the study of the longitudinal vibration behavior of the beam without taking into account the influence of the mass on the beam will be performed. Longitudinal vibrations of the beam may be described as axial vibrations of the beam. At first, the method of separation of variables will be applied to solve the longitudinal vibrations equation. The differential equation describing the longitudinal vibration of the spring-supported beam will be broken down into two differential equations where one is concerned with the time variable, whereas the other with the space variable. Following this, the boundary conditions of the springs will be applied to derive the characteristic equation.

Frequency equation

$$\tan(\lambda L) = \frac{2k(EA)\lambda}{(EA\lambda)^2 - k^2}.$$

4.4 Analytical Solution- Longitudinal Vibration (With Lumped Mass)

In addition, the analysis can also be extended to find the influence on the vibrations of a lumped mass that is attached at the centre of the beam. If there exists a lumped mass, the governing differential equation will be modified due to the introduction of an additional inertia force at the midpoint of the beam. The compatibility and equilibrium equations will be applied at the location of the lumped mass. Thus, the condition of continuity in the displacement along with the dynamic force from the mass will be taken into consideration. Hence, a new characteristic equation can be obtained based on the modified governing differential equation. By solving the equation, the new natural frequencies and mode shapes can be found for the longitudinal vibration of the beam with a lumped mass.

Frequency equation

$$-\mathrm{EA}\lambda\sin(\lambda\mathrm{L}) + (\mathrm{k_L} + \mathrm{k_R})\cos(\lambda\mathrm{L}) + \frac{\mathrm{k_L k_R}}{\mathrm{EA}\lambda}\sin(\lambda\mathrm{L})$$
$$-\mu\mathrm{S}(\lambda)\left[\mathrm{EA}\lambda^2\cos\left(\lambda(\mathrm{L}-\mathrm{a})\right) + \mathrm{k_R}\lambda\sin\left(\lambda(\mathrm{L}-\mathrm{a})\right)\right] = 0.$$

4.5 Analytical Solution- Transverse Vibration (No Lumped Mass)

Along with axial vibration, the transverse vibration of the beam is also taken into consideration. Transverse vibration is defined as the bending vibration of the beam around its longitudinal axis. The differential equation that governs transverse vibration can be obtained from the Euler-Bernoulli beam theory. Just like the axial vibration equation, the equation for transverse vibration is solved using separation of variables to obtain the space and time functions of the displacement. Boundary conditions associated with the springs can be used to derive the characteristic equation for transverse vibration.

Frequency equation

$$K(\beta)$$
$$= \begin{bmatrix} 1 & 0 & -1 & 0 \\ k_{LV} & EI\beta^3 & k_{LV} & -EI\beta^3 \\ \cosh\lambda & \sinh\lambda & -\cos\lambda & -\sin\lambda \\ EI\beta^3\sinh\lambda - k_{RV}\cosh\lambda & EI\beta^3\cosh\lambda - k_{RV}\sinh\lambda & EI\beta^3\sin\lambda - k_{RV}\cos\lambda & -EI\beta^3\cos\lambda - k_{RV}\sin\lambda \end{bmatrix}$$

For a non-trivial solution,

$$\det[\mathrm{K}(\beta)] = 0.$$

This determinant equation is the frequency equation.

4.6 Analytical Solution- Transverse Vibration (With Lumped Mass)

Beside the ones mentioned above, another way of further analysis of the transverse vibration could be through inclusion of the effect of the lumped mass at the centre of the beam. As with the case of longitudinal vibration, here the presence of the lumped mass means that there will be some inertia forces which will have to be considered while writing down the differential equation. Inclusion of the conditions for continuity of the deflections and the slopes of both segments of the beam at the point of attachment of the mass will provide a new equation having the mass parameter.

Frequency equation for symmetric modes

$$K_s(\beta) = \begin{bmatrix} 1 & 0 & -1 & 0 \\ k_{LV} & EI\beta^3 & k_{LV} & -EI\beta^3 \\ \sinh\lambda & \cosh\lambda & -\sin\lambda & \cos\lambda \\ 2EI\beta^3\sinh\lambda + m_d\omega^2\cosh\lambda & 2EI\beta^3\cosh\lambda + m_d\omega^2\sinh\lambda & 2EI\beta^3\sin\lambda + m_d\omega^2\cos\lambda & -2EI\beta^3\cos\lambda + m_d\omega^2\sin\lambda \end{bmatrix}$$

For a non-trivial solution, the determinant must vanish:

$$\det[\mathrm{K_s}(\beta)] = 0.$$

This is the symmetric frequency equation.

Frequency equation for Anti-symmetric modes

$$\mathrm{K_a}(\beta) = \begin{bmatrix} 1 & 0 & -1 & 0 \\ \mathrm{k_{LV}} & \mathrm{EI\beta^3} & \mathrm{k_{LV}} & -\mathrm{EI\beta^3} \\ \cosh\lambda & \sinh\lambda & \cos\lambda & \sin\lambda \\ \cosh\lambda & \sinh\lambda & -\cos\lambda & -\sin\lambda \end{bmatrix}.$$

The anti-symmetric frequency equation is therefore

$$\det[\mathrm{K_a}(\beta)] = 0.$$

This is the Anti-symmetric frequency equation.

4.7 Determine First Three Mode Shapes

With the analytical expression of the natural frequency obtained, the first three vibration mode shapes for the beam structure are obtained. The vibration mode shape is the particular way that the beam vibrates when deformed. Whereas the first vibration mode shape is associated with the first vibration mode of the beam, the second and third mode shapes correspond to the other modes of vibration. Mode shapes are essential because they provide the deformation pattern of the beam. In the present study, mode shapes are determined using the analytical approach to solving the differential equation. Graphical representations of the mode shapes are plotted. Additionally, the effects of the spring stiffness and lumped mass on the mode shapes are investigated.

I. Longitudinal vibration without lumped mass

The general mode-shape expression is

$$\mathrm{U_n}(\mathrm{x}) = \mathrm{A_n}\cos(\lambda_\mathrm{n}\mathrm{x}) + \mathrm{B_n}\sin(\lambda_\mathrm{n}\mathrm{x}).$$

Substituting the values of $\mathrm{A_n}$, $\mathrm{B_n}$ and λ_n for each mode:

Mode 1

$$U_1(x) = \cos(1.653911x) + 0.438772\sin(1.653911x)$$

Mode 2

$$U_2(x) = \cos(6.713945x) + 0.108087\sin(6.713945x)$$

Mode 3

$$U_3(x) = \cos(12.793574x) + 0.056723\sin(12.793574x)$$

II. Longitudinal vibration with lumped mass

Mode 1

$$U_1(z) = \cos(0.962121z) + 0.754260\sin(0.962121z) - 0.988657\,H(z-0.25)\sin\big(0.962121(z-0.25)\big).$$

Mode 2

$$U_2(z) = \cos(6.713866z) + 0.108088\sin(6.713866z) + 0 \cdot H(z-0.25)\sin\big(6.713866(z-0.25)\big).$$

Since $C_2 \approx 0$, this can be written more compactly as

$$U_2(z) = \cos(6.713866z) + 0.108088\sin(6.713866z).$$

Mode 3

$$U_3(z) = \cos(7.777092z) + 0.093311\sin(7.777092z) + 1.930219\,H(z-0.25)\sin\big(7.777092(z-0.25)\big).$$

III. Transverse vibration without lumped mass

The general mode-shape expression is

$$W_n(x) = A_n\cosh(\beta_n x) + B_n\sinh(\beta_n x) + C_n\cos(\beta_n x) + D_n\sin(\beta_n x).$$

The first three transverse mode shapes are:

Mode 1

$$W_1(x) = \cosh(\beta_1 x) - 0.9169247470\,\sinh(\beta_1 x) + \cos(\beta_1 x) + 698.8051713908\,\sin(\beta_1 x).$$

Mode 2

$$W_2(x) = \cosh(\beta_2 x) - 1.0038288653\,\sinh(\beta_2 x) + \cos(\beta_2 x) + 87.1849655534\,\sin(\beta_2 x).$$

Mode 3

$$W_3(x) = \cosh(\beta_3 x) - 0.9998254552\sinh(\beta_3 x) + \cos(\beta_3 x) + 25.5008007519\sin(\beta_3 x).$$

IV. Transverse vibration with lumped mass

Mode 1

$$\psi_1(z) = \cosh(4.284723969z) - 499.863811\sinh(4.284723969z) + \cos(4.284723969z) + 1700.574330\sin(4.284723969z).$$

Mode 2

$$\psi_2(z) = \cosh(12.520493156z) - 1.003829\sinh(12.520493156z) + \cos(12.520493156z) + 87.184965\sin(12.520493156z).$$

Mode 3

$$\psi_3(z) = \cosh(16.096693800z) - 0.086689\sinh(16.096693800z) + \cos(16.096693800z) + 41.415181\sin(16.096693800z).$$

4.8 ANSYS Finite Element Simulation

As part of validation for the results obtained from the analysis of the structure, the numerical simulation analysis was performed using ANSYS Workbench 2024 R1 software. To conduct this, an analytical model with the same dimensions and properties as the theoretical model was developed using suitable beam elements. The conditions of elastic support at the two ends of the beam were modeled by applying boundary conditions of spring stiffness, while a mass element was added in the centre of the beam to represent the lumped mass.

The accuracy of the solution was achieved by discretizing the beam using sufficient finite elements, particularly around the point where the effect of the loading was applied, namely the midspan. The boundaries were also specified such that movement is allowed only within the direction of vibration. Modal analysis was used to obtain the natural frequency of vibration and its respective mode shapes. Results of the simulation were then compared to the theoretical results, proving that the mathematical model was correct.

4.9 Compare Analytical VS ANSYS Results

This stage is the final part of the methodology, which involves verification of the analytical solutions against those obtained numerically by ANSYS software. This stage entails the

use of the natural frequency and mode shapes of the first three vibration modes in the comparison process. If there is an agreement between both solutions, then the analytical solution is considered accurate, which implies that the model can accurately describe the dynamics of the beam structure. Conversely, if there is any discrepancy, then it is essential to trace back the derivation process from the governing equation to the analytical solution stages.

4.10 System Description and Model

A schematics of the beam spring mass system model is depicted in Figure 2 that is similar to the one used in ANSYS software. In the proposed model, the beam is equipped with horizontal springs at the two ends to depict the stiffening effect of the supports in the longitudinal direction. In addition, the beam is equipped with vertical springs to depict the transverse stiffening effects.

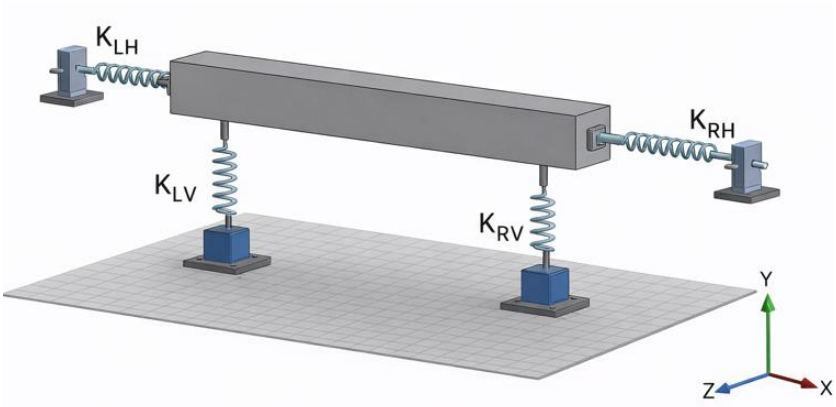

Figure 2 ANSYS-style schematic model of the beam supported by horizontal and vertical springs

Table 1 Main model parameters used in the analytical solution

Parameter	Variable (unit)	Value
Young's modulus	E (Pa)	6.89 × 10^10
Density	ρ (kg/m³)	2.8 × 10^3
Beam / rod length	L (m)	0.5

Cross-sectional area		A (m^2)	2 × 10^-4
Second moment of area		I (m^4)	1.677 × 10^-9
Spring Stiffness(For Symmetric Spring)		kLH, kRH, kLV, kRV (N/m)	1 × 10^7
Spring Stiffness(For Asymmetric Spring)	Right vertical spring stiffness	kRH, kRV (N/m)	1 × 10^8
	Left vertical spring stiffness	kLH, kLV (N/m)	1 × 10^5
Right vertical spring stiffness		(N/m)	1 × 10^7
Disc / lumped mass location		a = L/2 (m)	0.25
Disc area		Ad (m^2)	4 × 10^-4
Disc density		ρd (kg/m^3)	7800
Disc thickness		td (m)	0.160256
Disc mass		Md (kg)	0.5
Axial rigidity		EA (N)	1.378 × 10^7
Flexural rigidity		EI ($N·m^2$)	115.5453
Distributed mass per unit length		ρA (kg/m)	0.56
Axial wave speed		c (m/s)	4960.56
Non-dimensional mass ratio		μ	0.892857

CHAPTER 5. RESULTS & DISCUSSION

5.1 Longitudinal Vibration of the Symmetrical Spring-supported Beam without Lumped Mass

The Natural frequencies are

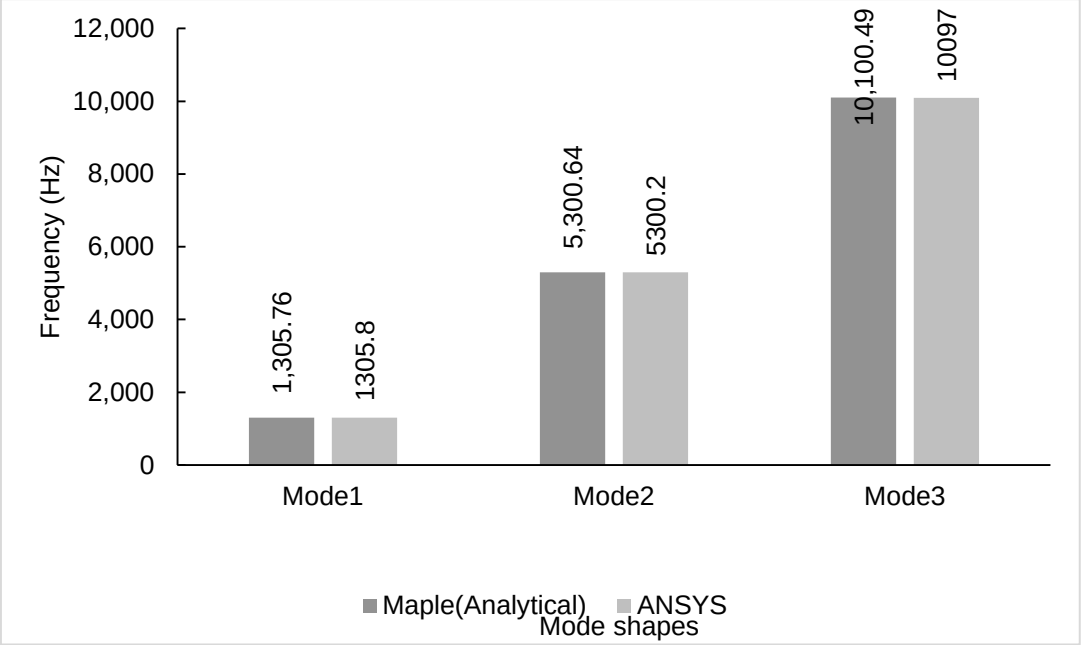

Figure 3. Frequency comparison of ANSYS and Maple

The natural frequencies obtained from the calculations of the beam when attached to the springs without the presence of any lumped mass at the centre of the beam are 1305.76 Hz, 5300.64 Hz, and 10100.49 Hz for the first, second, and third modes of axial vibration, respectively. These frequencies increase significantly with increasing mode numbers. Since the axial stiffness is proportional to EA, the axial frequencies will be much larger as compared to those of transverse frequencies. This means that there is more opposition to axial vibrations than transverse vibrations.

The frequency comparison shown in Figure 3 of the longitudinal vibrations of the spring-supported beam without a lumped mass is found to be very close for the first three modes of vibration. This is because the analytical solution with Maple and ANSYS solution result in the same value of frequency for the first mode, which is 1305.76 Hz for analytical and 1305.8 Hz for the ANSYS solution. Similarly, the analytical solution gives 5300.64 Hz while the numerical solution by ANSYS gives 5300.2 Hz for the second mode. For the third mode, the analytical frequency is 10100.49 Hz while the ANSYS solution frequency is

10097 Hz. This means that the difference is very minimal between the two solutions, especially in the higher-order modes due to discretization and numerical errors.

Interpretation of the First Three Axial Mode Shapes:

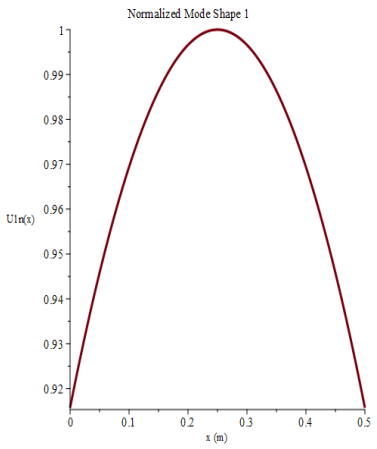

Maple output for First Mode Shape (Analytical)

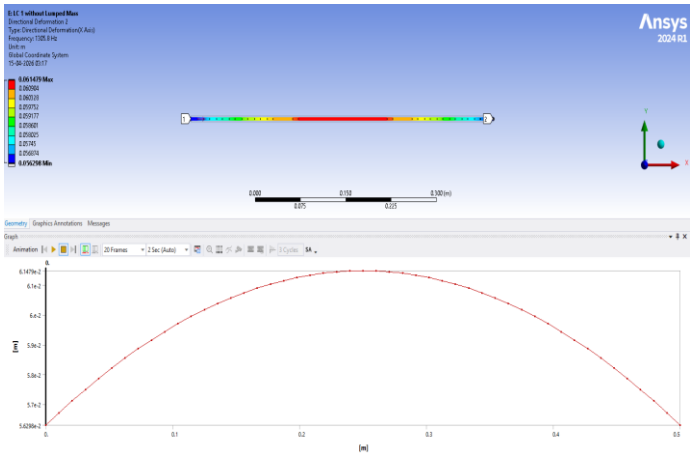

ANSYS validation for First Mode Shape

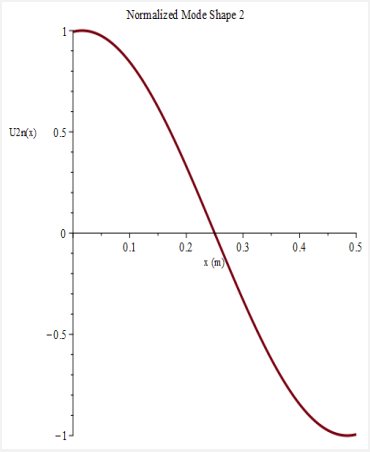

Maple output for Second Mode Shape (Analytical)

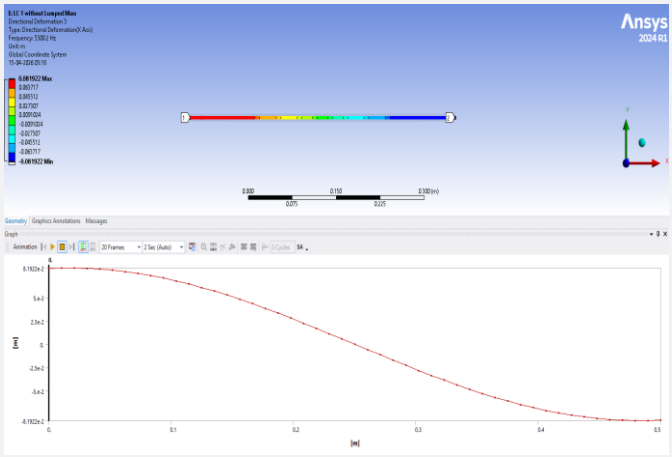

ANSYS validation for Second Mode Shape

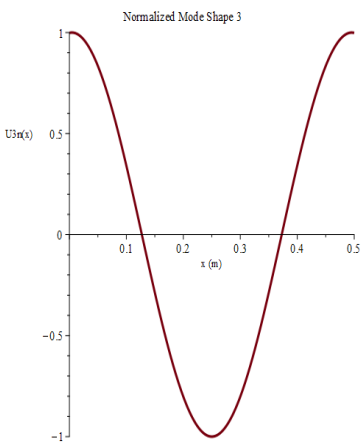

Maple output for Second Mode Shape (Analytical)

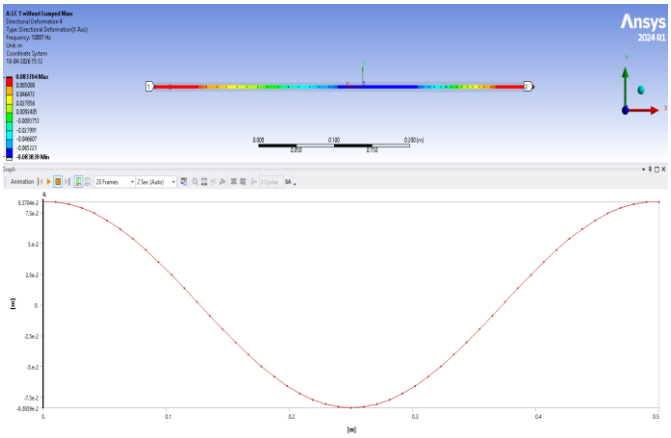

ANSYS validation for Third Mode Shape

Figure 4. Mode shape 1; Mode shape 2; Mode shape 3

The first three axial mode shapes of the spring-supported beam without a lumped mass show a clear progression in deformation complexity as the mode number increases. The first mode represents the fundamental global axial response, with a smooth symmetric deformation and no internal node, indicating that the entire beam vibrates in the same phase. The second mode introduces one internal nodal point where the displacement changes sign, dividing the beam into two regions vibrating in opposite phases. The third mode contains two internal nodes, creating three vibrating segments and demonstrating a shorter modal wavelength with higher spatial variation.

The first three longitudinal mode shapes of the beam with spring support, but without any lumped mass, derived from the ANSYS software are in complete conformity with those of the theory, as illustrated by the above Figure 4.

5.2 Longitudinal Vibration of the Symmetrical Spring-Supported Beam with Central Lumped Mass

The natural frequencies are

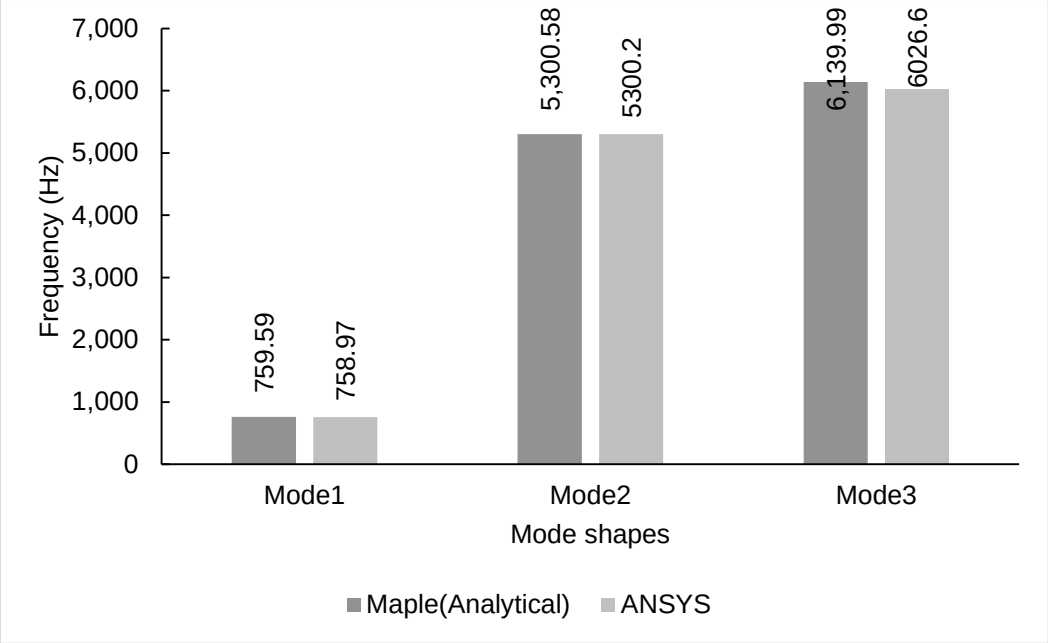

Figure 5. Frequency comparison of ANSYS and Maple

When heavy loads are attached to the middle point of the beam, then the frequency for the first three vibrations along the axis become 759.59 Hz, 5300.58 Hz, and 6139.99 Hz, respectively. From the above results, it can be noted that the frequency of the first and the third mode of vibration has reduced significantly, but the second mode of vibration has been slightly affected. From the above findings, it shows that the effect of heavy masses will differ according to the mode of vibration.

There is a very good comparison of the natural frequency value from analysis of 6139.99 Hz and the natural frequency value of ANSYS of about 6026 Hz. Though there is a big difference in the values obtained, this is still acceptable. The natural frequency of the mode increases with the increase in the number of modes in both cases, and both have taken into consideration the effect of the mass located at the centre. From the discussion above, one may conclude that there is good correlation between the analytical results and the numerical results.

Interpretation of Modified Axial Mode Shapes

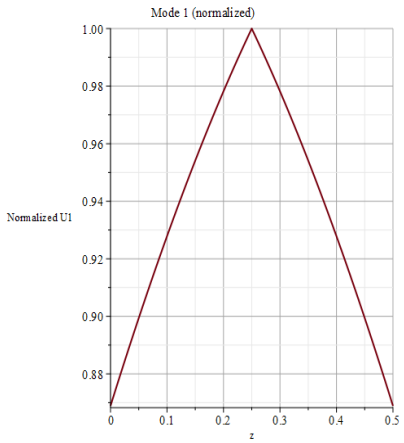

Maple Output for First Mode Shape (Analytical)

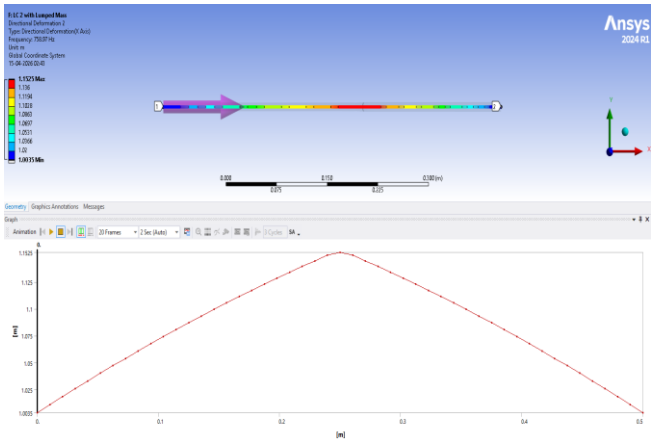

ANSYS validation for First mode shape

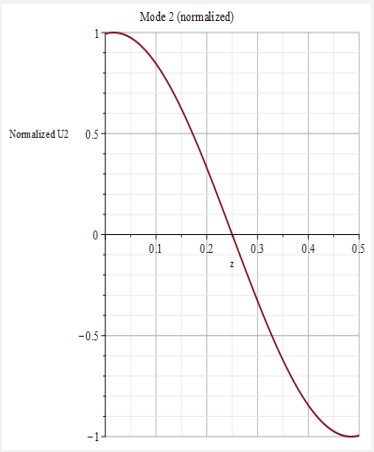

Maple Output for Second Mode Shape (Analytical)

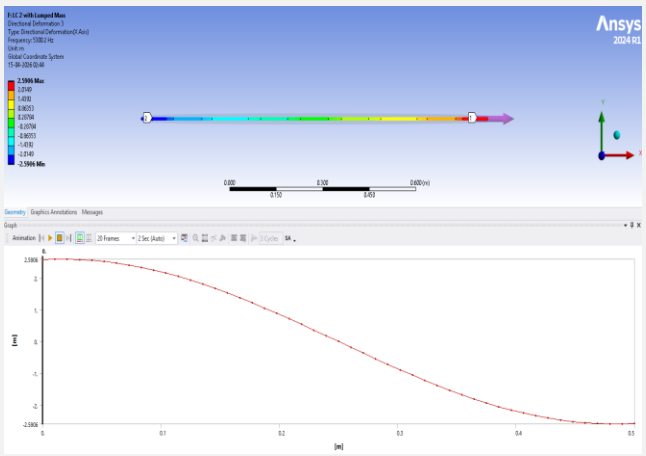

ANSYS validation for Second mode shape

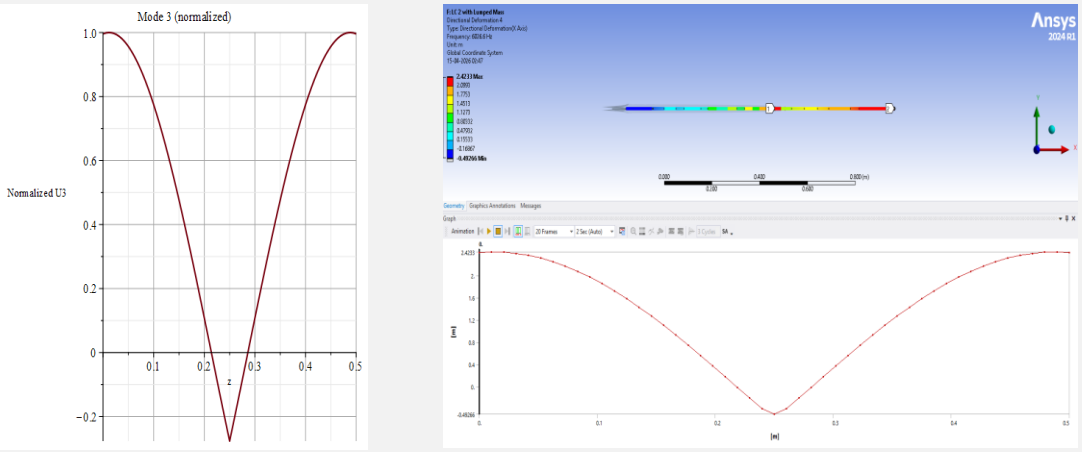

Maple Output for Second Mode Shape (Analytical)

ANSYS validation for Third mode shape

Figure 6. Maple generated Mode shape 1; Mode shape 2; Mode shape 3

From the analysis of the first three vibration modes for the case when the mass is attached to the midpoint of the spring-loaded beam, it follows that apart from the natural frequency values, also the vibration modes depend on the presence of an added mass. However, despite the fact that the first vibration mode is still symmetric with respect to the midpoint of the beam, which coincides with the location of the maximal displacements for the first vibration mode, the shape of the mode is largely defined by the midpoint of the beam, where the mass is placed. The second mode is characterized by an antisymmetric shape with a node being at the midpoint of the beam. As a result, due to the absence of displacements in this mode around the midpoint of the beam, the added mass does not significantly affect the shape of the vibration mode.

The first three longitudinal mode shapes of the beam with spring support with lumped mass at centre, derived from the ANSYS software are in complete conformity with those of the theory, as illustrated by the above Figure 6.

5.2.1 Comparative Discussion of Longitudinal Vibration Results

In comparing the longitudinal frequencies of both modes, it is seen that the first mode decreases by approximately 41.83%, the second one remains the same, while the third one decreases by approximately 39.21%. It shows that the effect of additional mass is dependent on the contributions made by the mode at the centre of the beam instead of being dependent on mass only. The first mode is highly sensitive because of its high displacement at the centre, the second mode is insensitive because the centre lies in the transition area of the

modal, while the third mode is again sensitive due to higher displacement at the centre. From the theoretical point of view, the additional mass contributes to increased generalized inertia, while there is no change in stiffness.

Table 2 Comparison of longitudinal natural frequencies with and without central lumped mass

Mode	Without Mass (Hz)	With Mass (Hz)	Change (%)
1	1305.76	759.59	-41.83
2	5300.64	5300.58	~0.00
3	10100.49	6139.99	-39.21

5.3 Transverse Vibration of the Symmetrical Spring-supported Beam without Lumped Mass

5.3.1 Analytical Solution

The analytical frequencies are

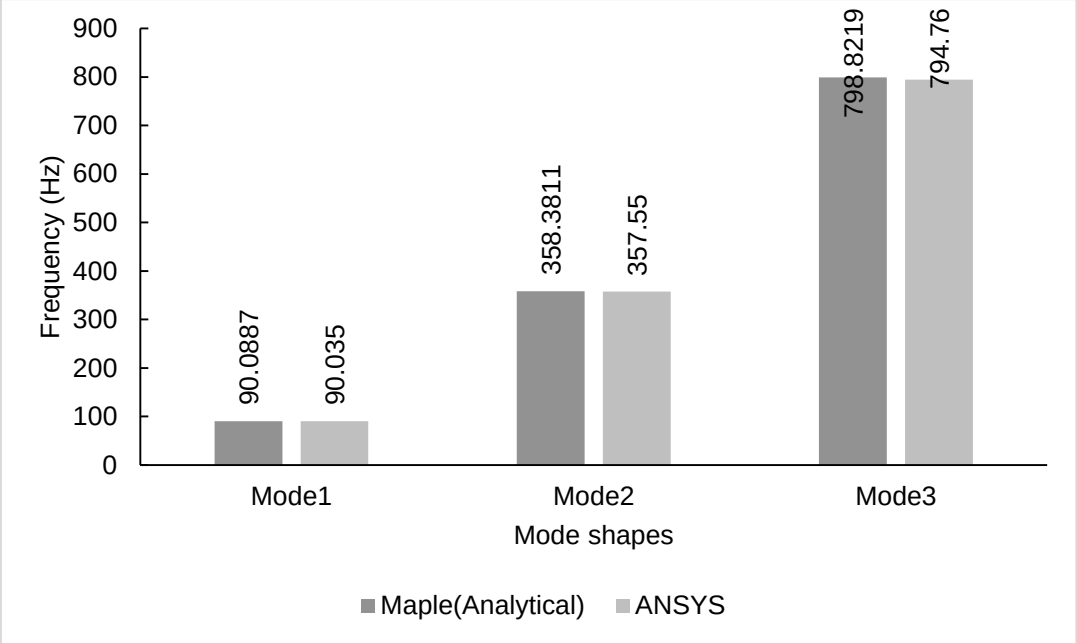

Figure 7. Frequency comparison of ANSYS and Maple

For the spring-supported beam without a lumped mass, the first three transverse natural frequencies are 90.0887 Hz, 358.3811 Hz, and 798.8219 Hz, which are much lower than

the corresponding axial frequencies because the flexural stiffness EI is significantly smaller than the axial stiffness EA in a slender beam. The first mode represents the fundamental bending response, while the second and third modes show progressively more complex flexural patterns with one and two internal sign changes, respectively. The nonlinear spacing of these frequencies reflects the fourth-order Euler–Bernoulli beam behavior together with the influence of elastic end springs, which provide less restraint than perfectly fixed supports and therefore reduce the frequencies. From a practical standpoint, bending vibration is more flexible and more likely to control service-level resonance, making the first transverse mode the most critical under low-frequency excitation, while higher modes become important under broadband or high-speed loading.

Both analytical and numerical simulation methods shows the increase in fequency with an increase in modes and account for the influence of elastic boundary conditions on the bending behavior. The extremely good match between both methods validates the accuracy of the analysis and ANSYS modeling in calculating the transverse dynamic response of the beam resting on springs with no mass in its middle point.

Interpretation of the First Three Transverse Mode Shapes

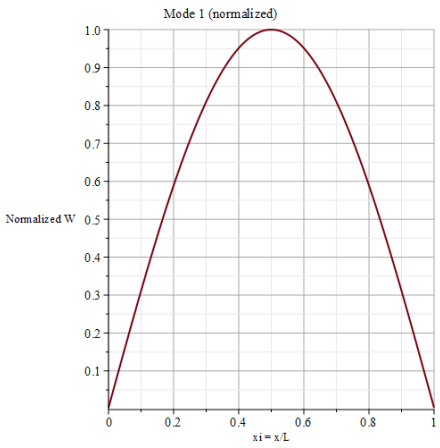

Maple Output for First Mode Shape (Analytical)

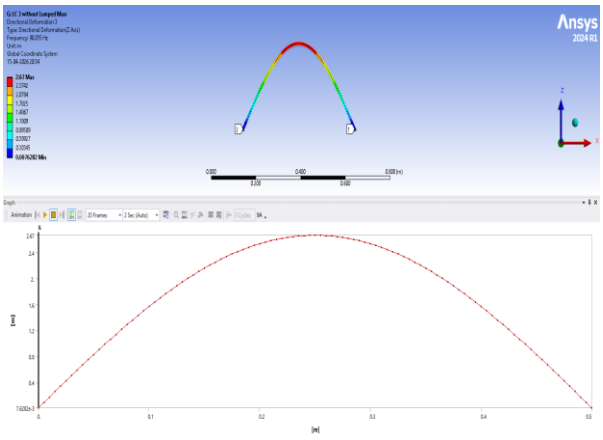

ANSYS validation for first mode shape

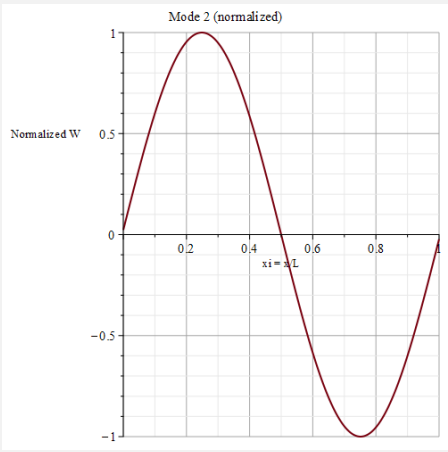

Maple Output for Second Mode Shape (Analytical)

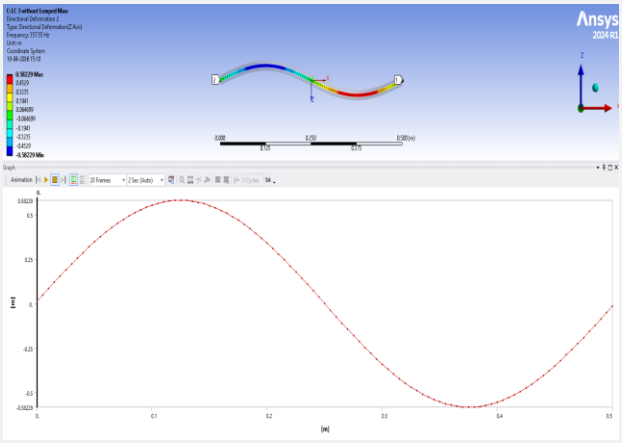

ANSYS validation for second mode shape

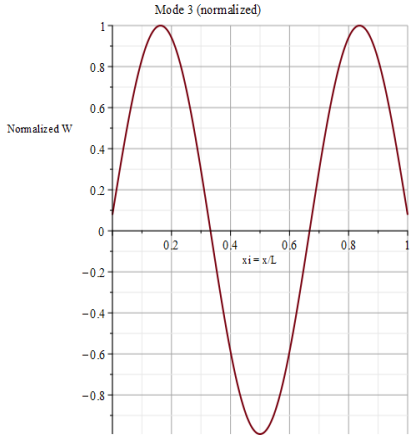

Maple Output for Third Mode Shape (Analytical)

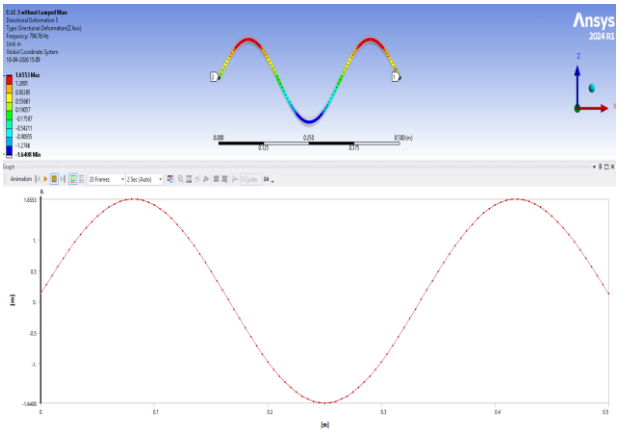

ANSYS validation for third mode shape

Figure 8. Maple generated a. Mode shape 1; Mode shape 2; Mode shape 3

It is clear from the above results that the first three transverse modes of vibration of the beam loaded by elastic springs without any further loads correspond to the natural pattern of bending vibrations. In addition, there is a growth of modal complexity in the higher order modes. Namely, the first transverse mode is a symmetrical bending mode with the peak deflection of the beam achieved in its middle point; hence, this mode has the largest deflections and is considered the most essential mode. At the same time, the second mode of vibration has a single node on the beam that divides it into two bending areas. Thereby, the third transverse mode contains two nodes and corresponds to three bending segments

of the beam. Higher-order transverse modes become important only under excitation of higher frequency loads. The usage of elastic springs as the boundary condition implies that the ends of the beam have some freedom and cause slight softening of the system. It should be emphasized that the analysis of transverse modes allows detecting regions with maximal deflections and maximal curvatures of the beam.

The first three transverse mode shapes of the beam with spring support without lumped mass at centre, derived from the ANSYS software are in complete conformity with those of the theory, as illustrated by the above Figure 8.

5.4 Transverse Vibration of the Symmetrical Spring-supported Beam with Central Lumped Mass

The natural frequencies are

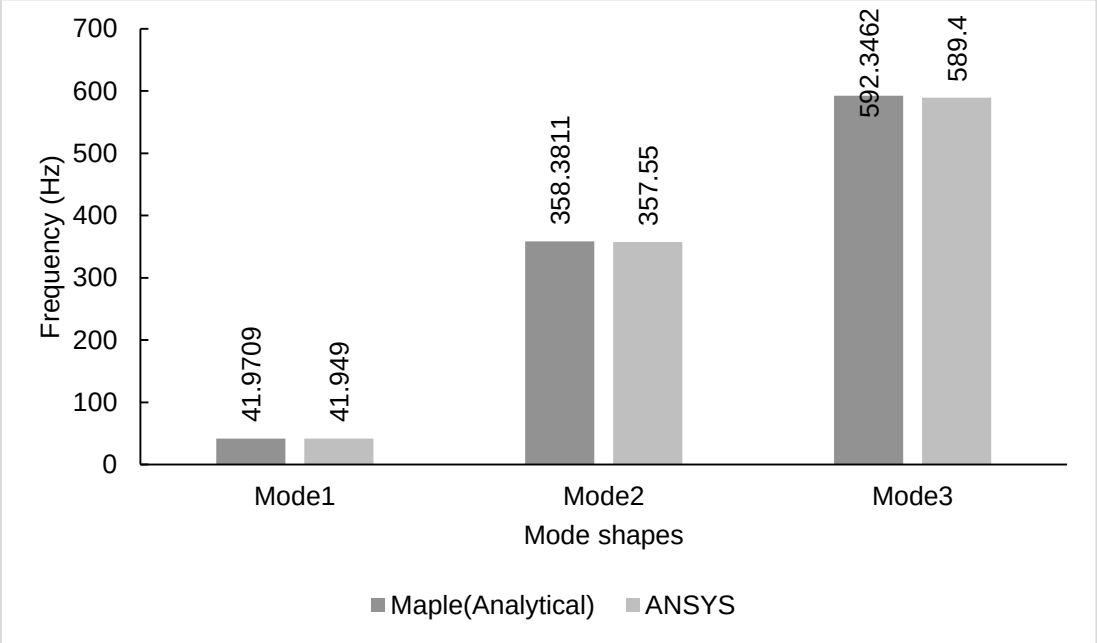

Figure 9. Frequency comparison of ANSYS and Maple

Regarding the situation where there is a concentrated mass located at the centre of the beam, the first three bending frequencies are determined to be 41.970869 Hz, 358.381127 Hz, and 592.346226 Hz respectively. Particularly, there is a decrease in frequency in the first bending mode by 53.41%, no changes in the frequency in the second mode, and reduction of the third bending mode frequency by 25.85%. There is a very strong influence of the concentrated mass at the beam centre on symmetric modes of vibrations, but none or minimal influence on the antisymmetric mode. From the Figure 9, we can conclude that there is good correlation between the analytical results and the numerical results.

Interpretation of modified transverse mode shapes

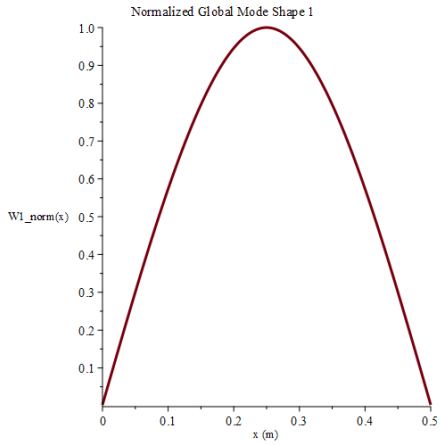

Maple Output for First Mode Shape (Analytical)

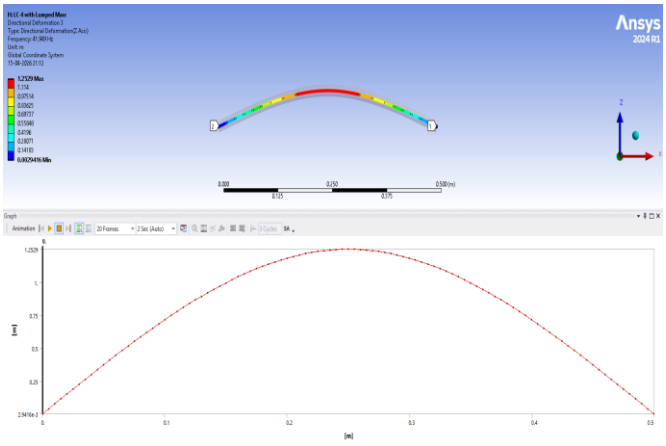

ANSYS validation for first mode shape

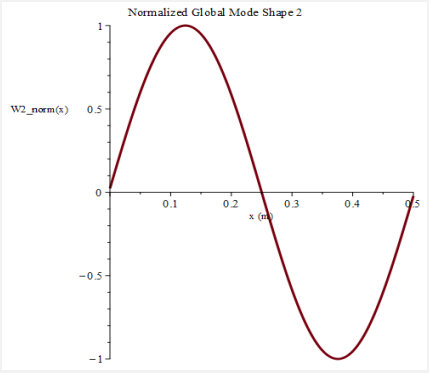

Maple Output for Second Mode Shape (Analytical)

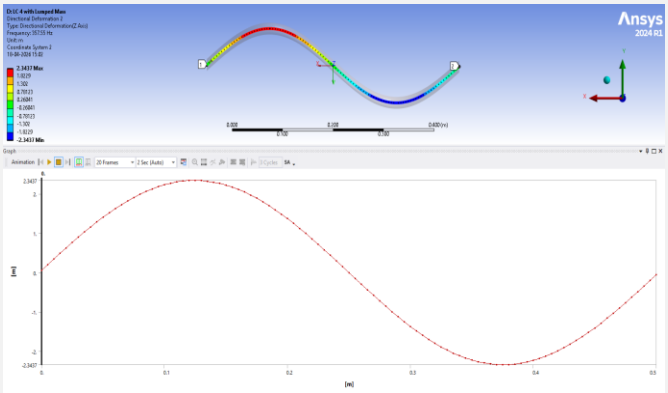

ANSYS validation for second mode shape

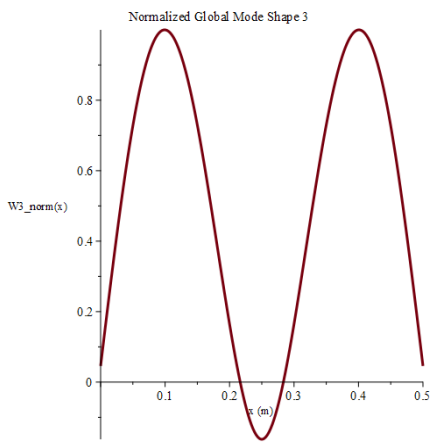

Maple Output for Third Mode Shape (Analytical)

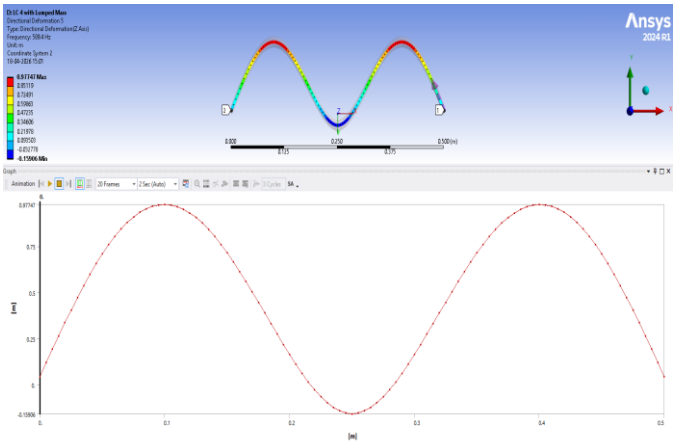

ANSYS validation for third mode shape

Figure 10. Maple generated Mode shape 1; Mode shape 2; Mode shape 3

Mode shapes 1 to 3 of the spring supported beam with a central lumped mass show the influence of mode shapes on the presence of the attached lumped mass. The mode shape of the first mode of vibration is the symmetric mode shape with maximum deformation at mid-span. This suggests that there is full participation of the lumped mass together with reduced natural frequencies due to increased inertia. Conversely, the mode shape of the second mode of vibration is the anti-symmetric mode shape with zero deformation at the centre. This shows that the centre has now become a node of the mode shape. As a result, the lumped mass is dynamically inactive, hence very minimal effect of the mass in this mode shape. The mode shape of the third mode of vibration takes on another high order symmetric mode shape with side maximum deformations and central minimum deformations. This implies that the centre and the lumped mass both contribute to the vibration characteristics.

The first three transverse mode shapes of the beam with spring support without lumped mass at centre, derived from the ANSYS software are in complete conformity with those of the theory, as illustrated by the above figure 10.

5.4.1 Comparative Discussion of Transverse Vibration Results

By comparing the transverse natural frequencies of systems with and without mass added at the centre, it can be seen that only the first and third frequencies are reduced, while the second frequency remains unaffected. This shows that bending vibration is highly

susceptible to the presence of extra inertia at locations where modal amplitudes are large. The first frequency is affected to a greater extent because the bending motion is most prominent in the middle part, whereas the second frequency is symmetrical with a nodal point at the centre. Thus, the presence of the added mass has no influence on the inertia at the nodal point.

Table 3. Comparison of transverse natural frequencies with and without central lumped mass

Mode	Without Mass (Hz)	With Mass (Hz)	Change (%)
1	90.0887	41.9709	-53.41
2	358.3811	358.3811	~0.00
3	798.8219	592.3462	-25.85

5.5 Longitudinal Vibration of the Asymmetric Spring-supported Beam without Lumped Mass

The natural frequencies are

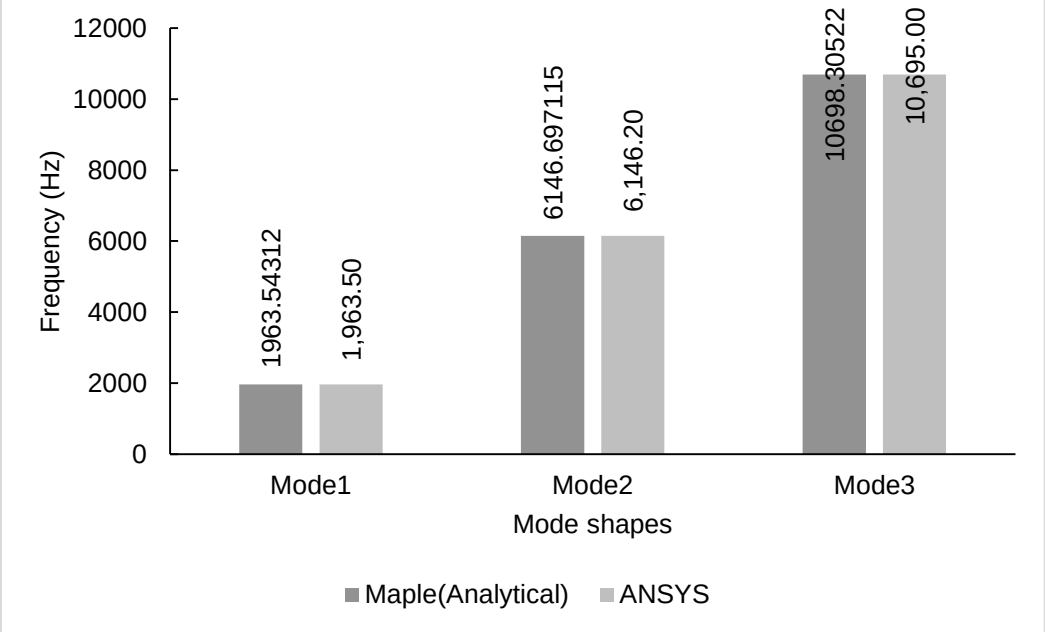

Figure 11. Frequency comparison of ANSYS and Maple

For longitudinal vibration of the non-symmetric spring supported beam without a lumped mass, the first three frequencies are 1963.54 Hz, 6146.69 Hz, and 10698.30 Hz. It is evident

from the data that a big jump occurs in the frequency value with an increasing mode number. This conforms to the expected trend for an axially restrained continuous system where the higher modes have shorter wavelengths and consequently axial strain energies. The high values also confirm the dynamic stiffness property of the beam for longitudinal vibration. Unlike the beam with symmetrical spring support, in which the two ends have similar boundary conditions, in the present case the ends have different supports, and therefore eigenvalues differ accordingly.

The comparison of the longitudinal vibration of the asymmetric spring supported beam without the lumped mass further proves that the theoretical model, which was developed with the help of the Maple program, is also accurate enough since there is only a negligible difference between the theoretical results that were obtained with the help of the Maple program and the results obtained with the help of the ANSYS program as seen in figure 11. It should be noted that the difference between these two sets of results is insignificant, although it is more noticeable in the high mode due to the influence of numerical approximation and discretization. It is due to the fact that the higher mode implies a higher natural frequency, and the role of springs of different stiffnesses mounted at both ends of the beam should not be ignored.

Interpretation of the First Three Axial Mode Shapes:

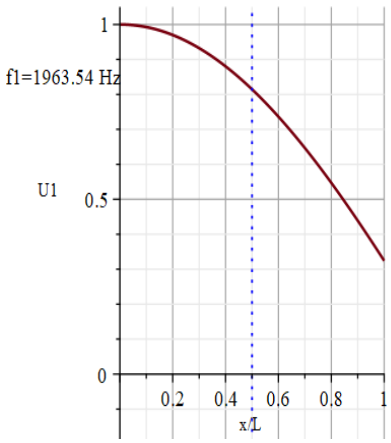

Maple Output for First Mode Shape (Analytical)

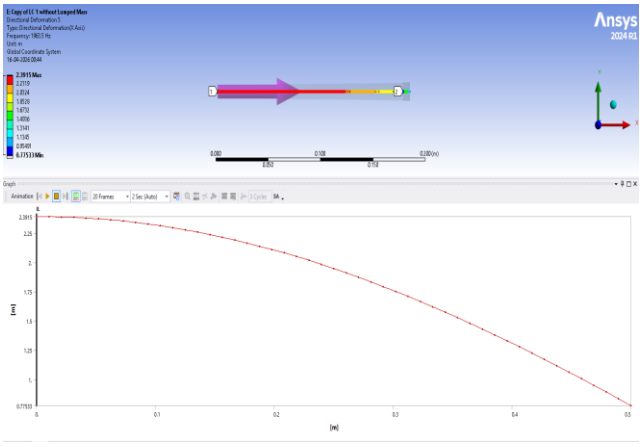

ANSYS validation for first mode shape

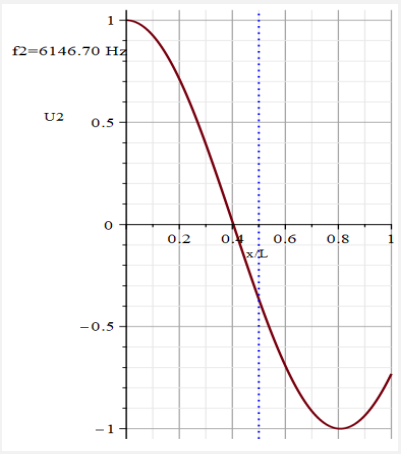

Maple Output for Second Mode Shape (Analytical)

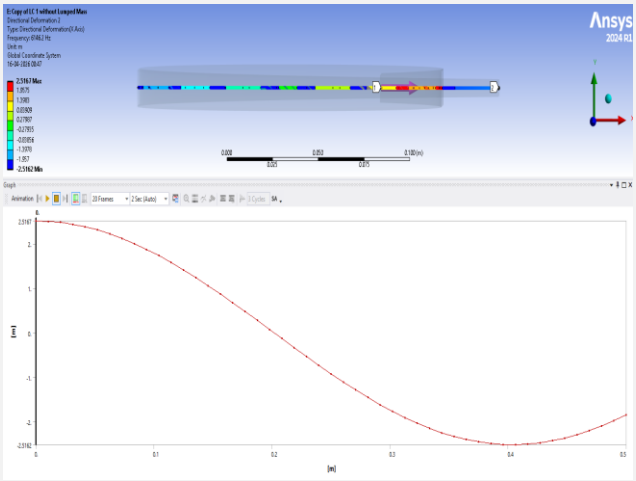

ANSYS validation for second mode shape

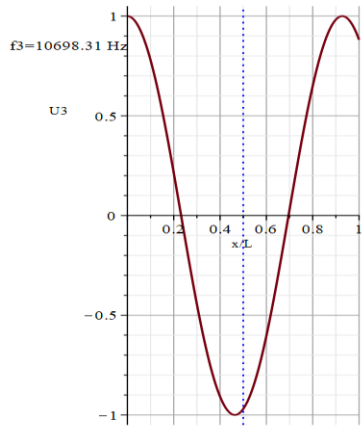

Maple Output for Third Mode Shape (Analytical)

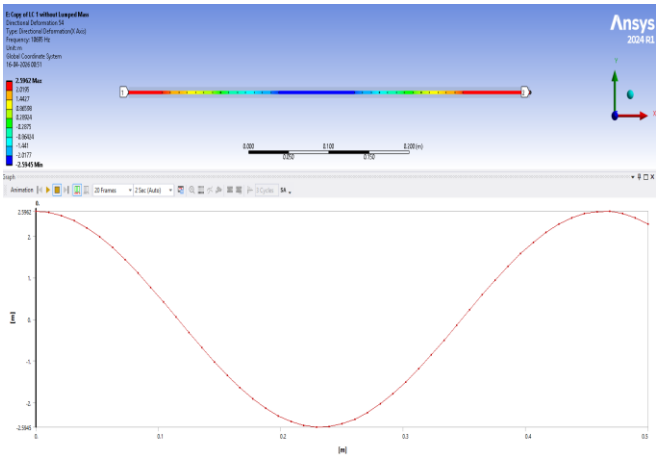

ANSYS validation for third mode shape

Figure 12.Mode shape 1; Mode shape 2; Mode shape 3

As follows from the results obtained by using ANSYS, the first three longitudinal modes of vibration for the asymmetric spring-supported beam that have not got any additional mass nodes demonstrate the highest similarity to their theoretical counterparts, and thus prove the validity of the proposed mathematical model. In its turn, the first mode represents the first global mode of vibration without any node inside, but features some degree of asymmetry as the result of unequal conditions of attachment at its edges (in the form of different springs). With regards to the second mode, it is represented by one node and two oppositely vibrating zones, while the third one is characterized by two nodes and three

zones. It should be emphasized, however, that in all those cases, the position of nodal lines and values of displacements differ slightly when compared to the corresponding symmetric example due to the effect exerted by different levels of restrains at the edge points as seen in Figure 12 .

5.6 Longitudinal Vibration of the Asymmetric Spring-Supported Beam with Central Lumped Mass

5.6.1 Analytical Solution

The natural frequencies are

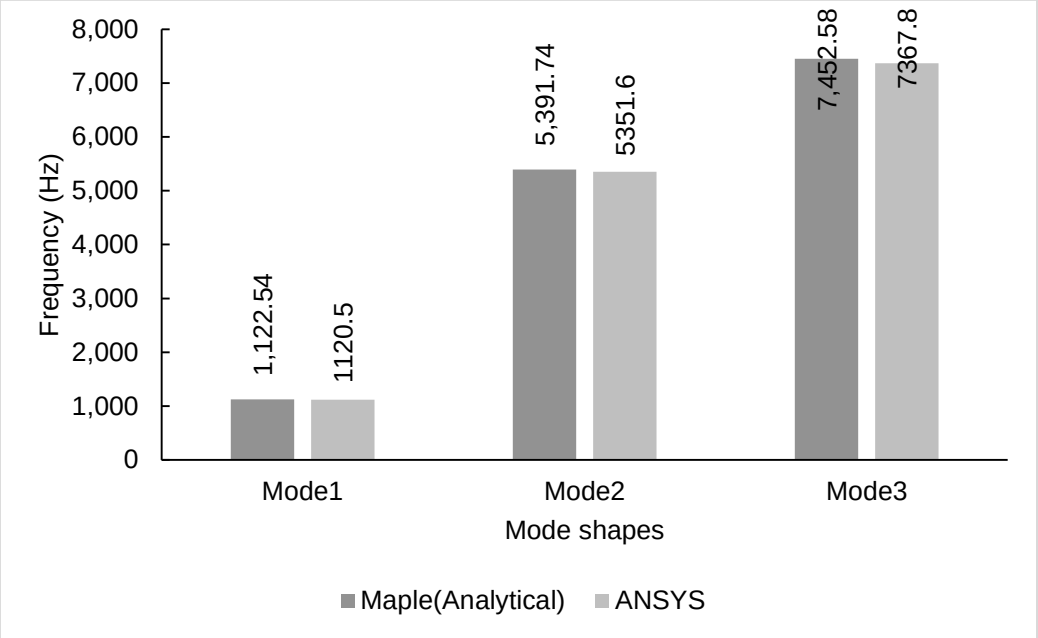

Figure 13. Frequency comparison of ANSYS and Maple

In terms of frequency comparison of longitudinal vibration of an asymmetric spring supported beam with concentrated mass located at its centre, the result of the analytical solution through Maple software and ANSYS is satisfactory as seen in figure 13. The first and second modes were observed to have high correlation with slight variations in their values, indicating that the formula was able to capture the influence of both the asymmetric beam and the additional concentrated mass. However, the third mode exhibited remarkable differences in the analysis. It is expected because the higher modes are more sensitive to finite elements as well as other factors like local inertia.

On the other hand, the difference in the third mode can be anticipated because high-order modes are more sensitive to meshing, approximations, and inertia. Both methods are able to accurately represent the trend of increase in frequencies along with the increase in mode

order and impact of the mass on the frequency of each particular mode. Therefore, this comparison proves that the analytical model used to estimate the longitudinal dynamics of the mass-loaded beam has been developed effectively.

Interpretation of Modified Axial Mode Shapes.

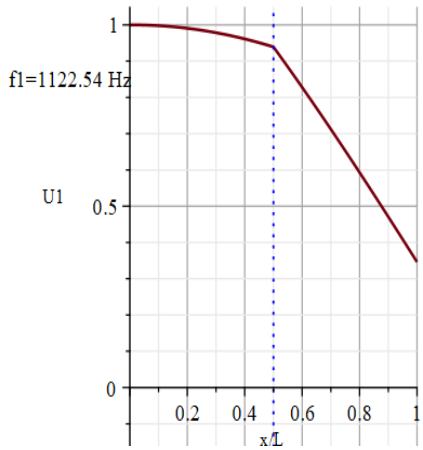

Maple Output for First Mode Shape (Analytical)

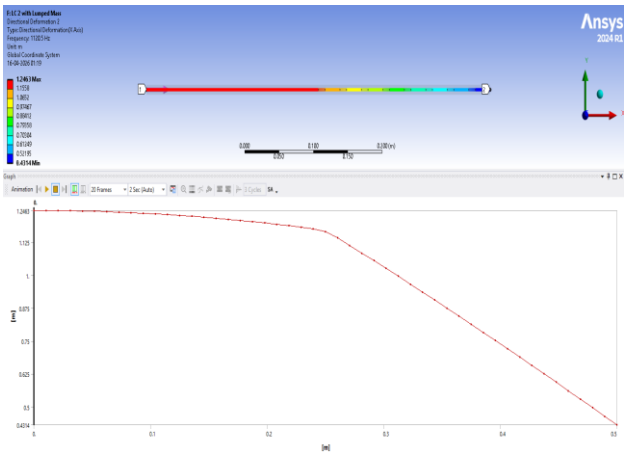

ANSYS validation for First mode shape

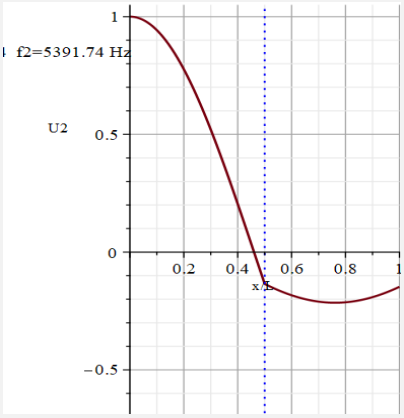

Maple Output for Second Mode Shape (Analytical)

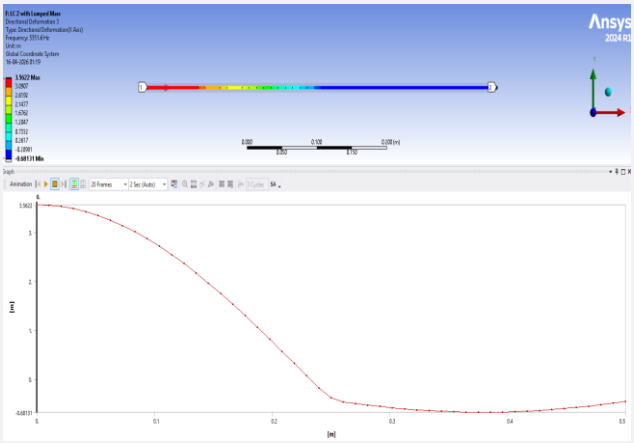

ANSYS validation for Second mode shape

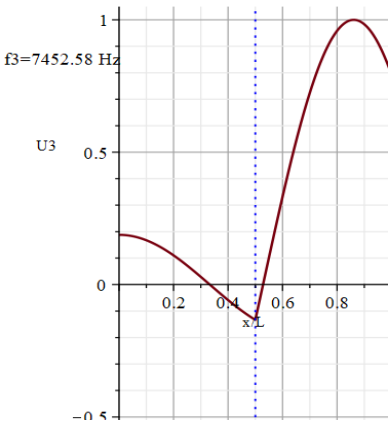

Maple Output for Third Mode Shape (Analytical)

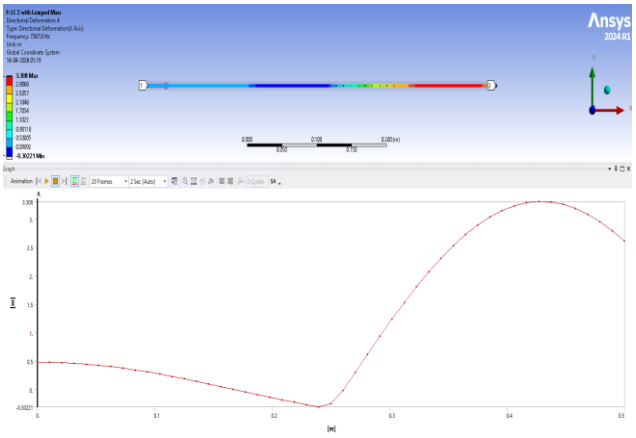

ANSYS validation for Third mode shape

Figure 14. Maple generated Mode shape 1; Mode shape 2; Mode shape 3

Natural frequencies of the unsymmetrical beam system with a central lumped mass are found to be in an increasing trend with respect to mode number, which is a characteristic feature of all continuous systems. The effect of the various spring stiffnesses and lumped mass at the centre point of the beam plays an important role in the dynamics of the system. From the results obtained, it is found that the first mode gets significantly influenced due to the presence of the midspan lumped mass..

The mode shapes used for comparison also verifies on these factors. The first mode shape includes axial deformation of the entire structure with an unbalanced shape and distinct centre impact. On the other hand, the second mode includes only one node located between the springs, dividing the beam into two parts with opposite vibrations. The third mode has two nodes representing a complex structure consisting of three segments. However, all curves remain continuous without any symmetry, given that the spring arrangement is unbalanced and the centre has inertia.

The first three transverse mode shapes of the beam with spring support without lumped mass at centre, derived from the ANSYS software are in complete conformity with those of the theory, as illustrated by the above figure 14.

5.6.2 Comparative Discussion of Longitudinal Vibration Results

Regardless of the mode considered, the decrease in frequency always occurs depending on the displacement of the point of maximal displacement that is the centre of the beam where

the concentrated mass is located. As for Mode 1, it is seen that the maximum decrease in the frequency is achieved since the first axial mode is a global deformation mode featuring significant displacements at the middle point of the beam, therefore the concentrated mass significantly increases the generalized inertia of the system. As for Mode 2, the decrease in frequency is not as significant since the displacements of the middle point of the beam are minimal, therefore the mass acts only actively in the vibrations.

Table 4 Comparison of longitudinal natural frequencies with and without central lumped mass

Mode	Without Mass (Hz)	With Mass (Hz)	Change (%)
1	1963.54	1,122.54	-42.83
2	6146.69	5,391.74	-12.28
3	10698.30	7,452.58	-30.33

5.7 Transverse Vibration of the Asymmetric Spring-supported Beam without Lumped Mass

5.7.1 Analytical Solution

The natural frequencies are

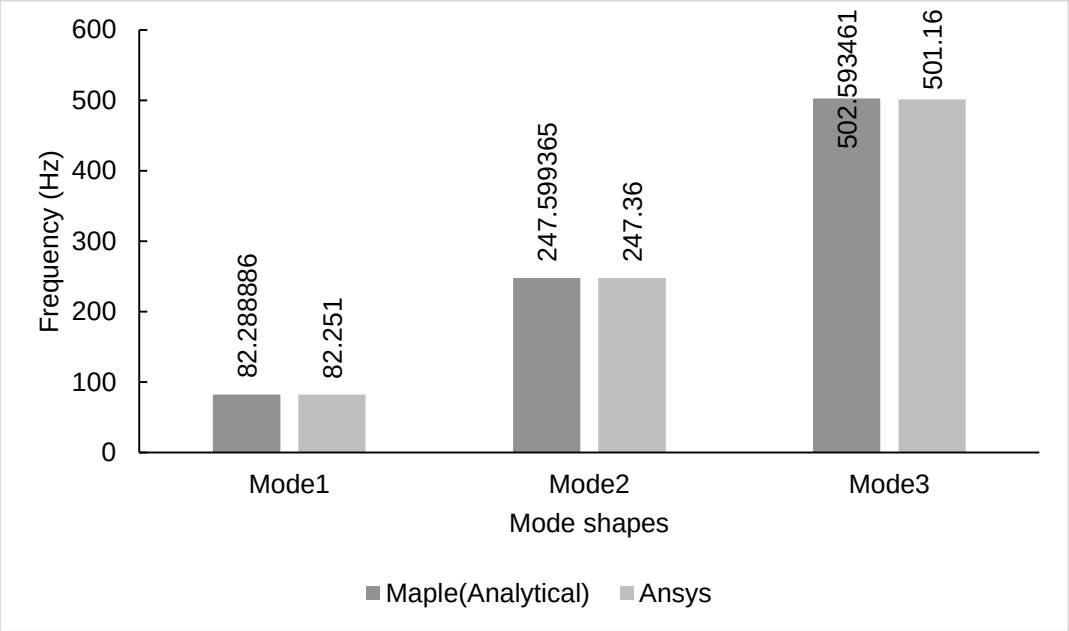

Figure 15. Frequency comparison of ANSYS and Maple

The comparison of the frequencies for the transverse vibrations of the beam resting on the springs without a lumped mass exhibits a high degree of consistency in the results obtained analytically using Maple and numerically using ANSYS as seen in figure 15. The differences observed in the calculation results of both approaches are quite small and are acceptable within engineering tolerances; however, they are larger for the higher mode due to the nature of the finite element method and numerical integration. In addition, both approaches show identical tendencies in an increasing trend of the frequencies with an increasing number of the mode and in the influence of different stiffness of the beams supporting the ends of the beam.

Interpretation of the First Three Transverse Mode Shapes

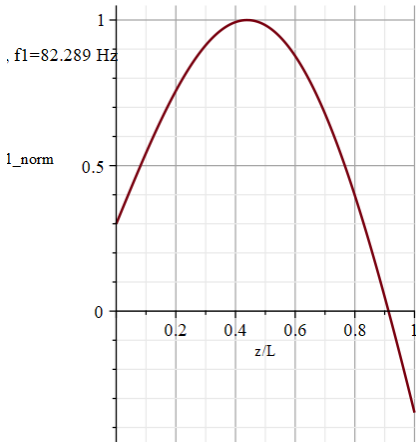

Maple Output for First Mode Shape (Analytical)

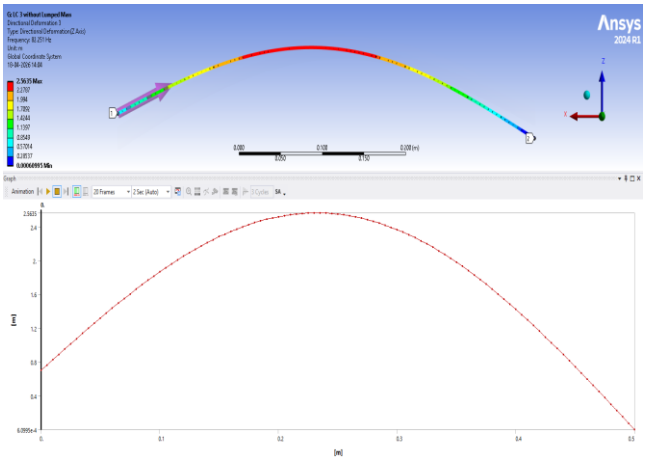

ANSYS validation for First mode shape

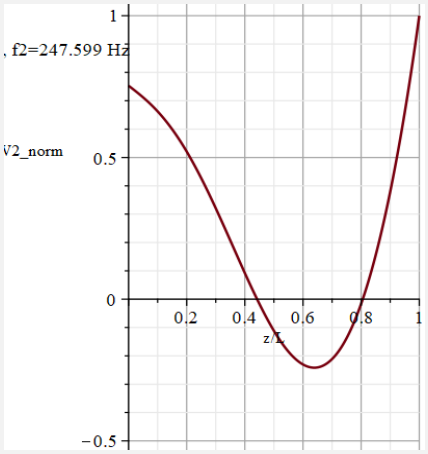

Maple Output for Second Mode Shape (Analytical)

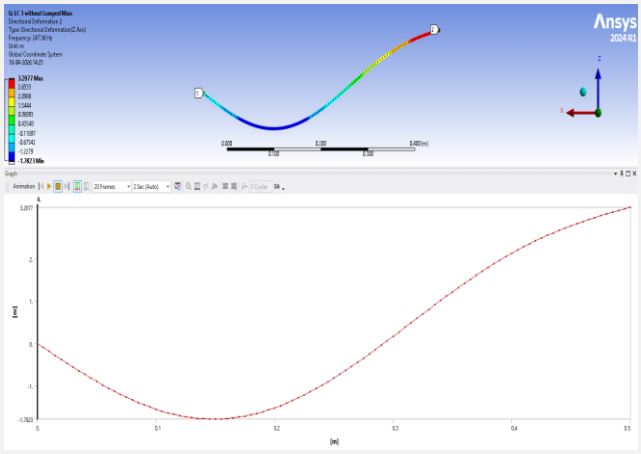

ANSYS validation for Second mode shape

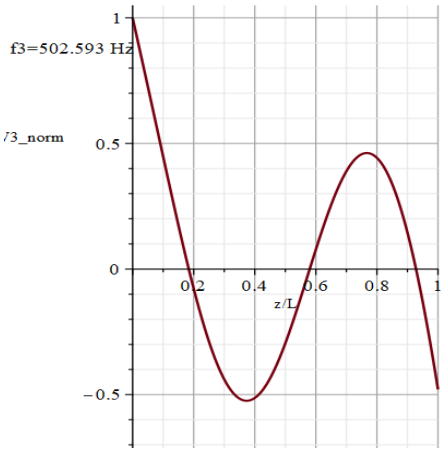

Maple Output for Third Mode Shape (Analytical)

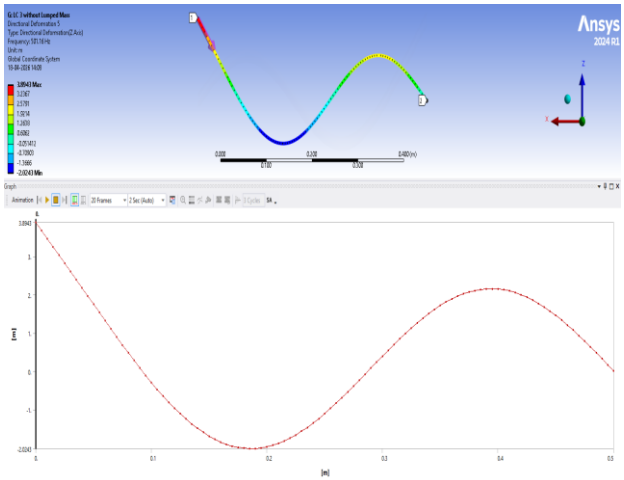

ANSYS validation for Third mode shape

Figure 16. Mode shape 1; Mode shape 2; Mode shape 3

The shapes of the modes also indicate the effect of asymmetry of the supporting condition. The first mode represents overall bending, for which the point of maximum deflection is not symmetrical. Moreover, the second and third modes include one and two nodes respectively, and have complex deflection patterns. Nonetheless, all the deflection patterns remain smooth and continuous, although they are asymmetrical with respect to the mid-point of the beam.

The first three transverse mode shapes of the beam with spring support without lumped mass at centre, derived from the ANSYS software are in complete conformity with those of the theory, as illustrated by the above Figure 16.

5.8 Transverse Vibration of the Asymmetric Spring-supported Beam with Central Lumped Mass

The natural frequencies are

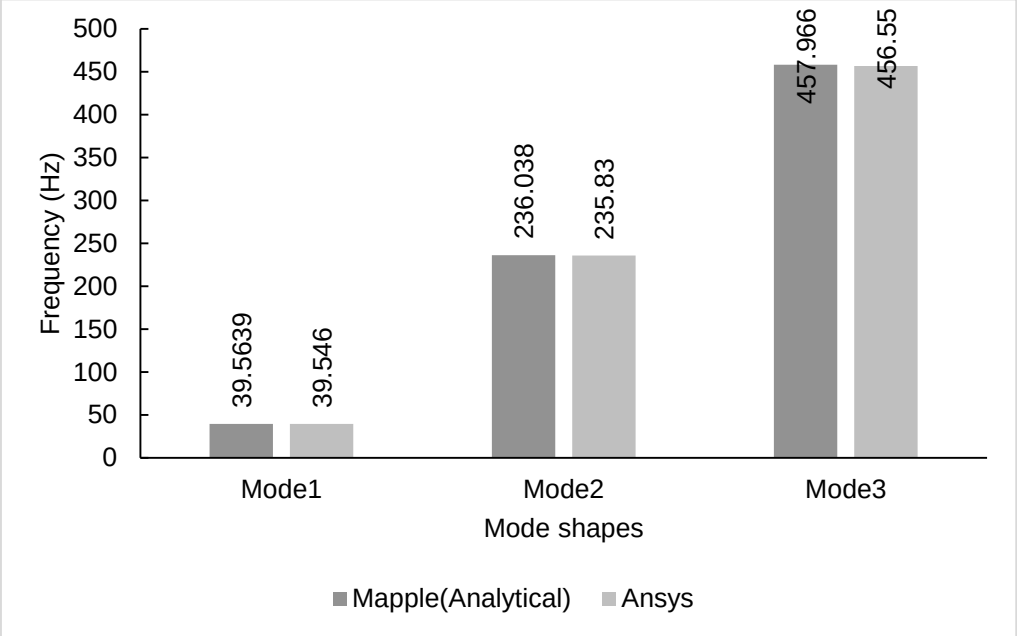

Figure 17. Frequency comparison of ANSYS and Maple

Comparison of the frequency of analytical solution of the Maple software package with the numerical analysis of ANSYS demonstrates a significant correlation factor in all three cases of natural vibration modes as seen in Figure 17. The deviation of frequencies obtained using both methods is very insignificant, indicating that the right equations, boundary conditions, and lumped mass method have been applied in both cases. Therefore, it can be concluded that the mathematical model developed to analyze transverse vibrations of the asymmetric beam is correct.

Interpretation of modified transverse mode shapes

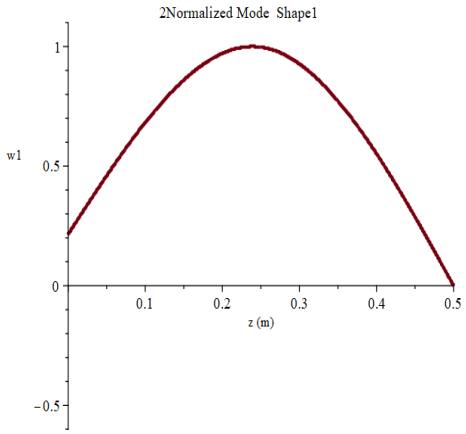

Maple Output for First Mode Shape (Analytical)

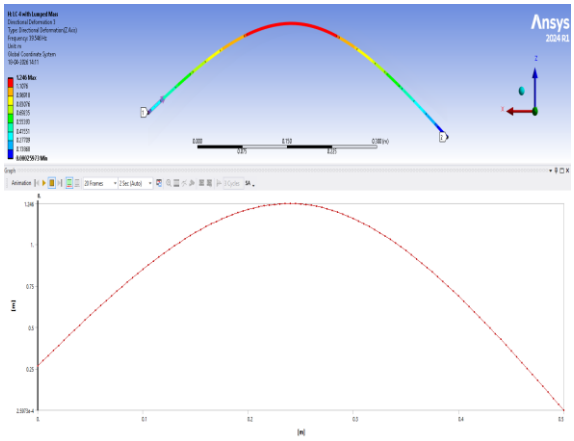

ANSYS validation for First mode shape

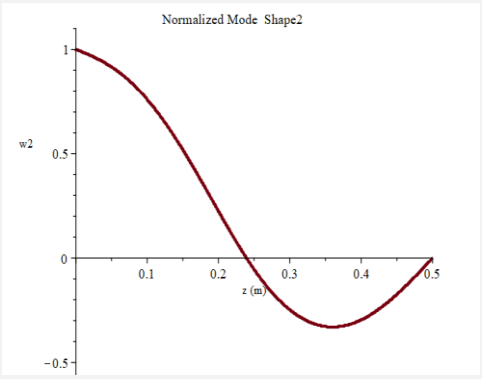

Maple Output for Second Mode Shape (Analytical)

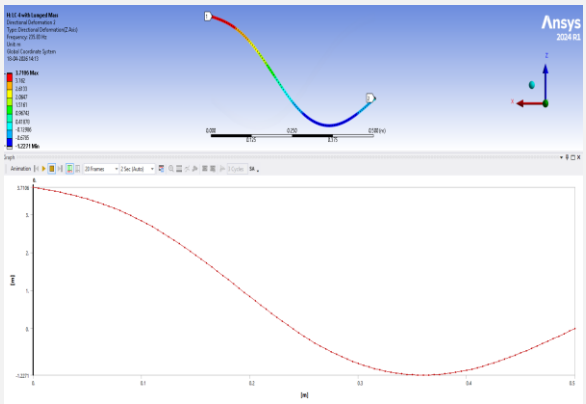

ANSYS validation for Second mode shape

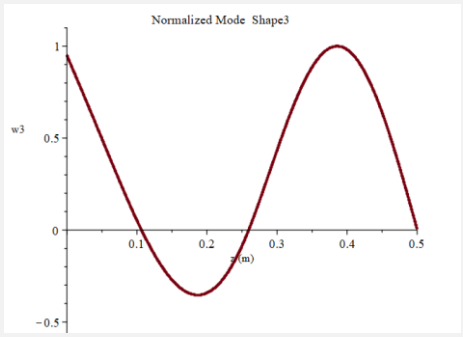

Maple Output for Third Mode Shape (Analytical)

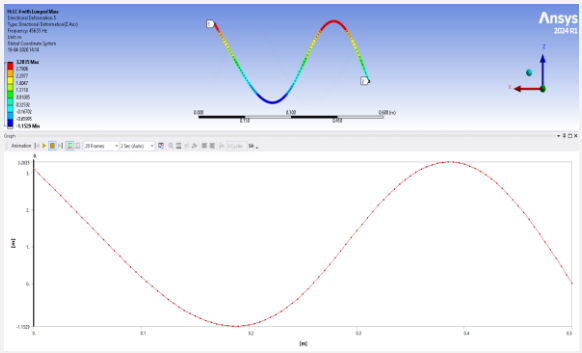

ANSYS validation for Third mode shape

Figure 18. Maple generated. Mode shape 1; Mode shape 2; Mode shape 3

The modal shapes from the ANSYS software simulation for the case of the transverse vibrations of the asymmetrically supported beam with the central concentrated mass coincide quite well with those calculated analytically from Maple mathematical software in respect of mode shapes and deformation pattern. Specifically, the mode one represents the fundamental shape of bending characterized by the single curvature with the maximum deflection located at the middle point of the span, which is the fundamental vibrational mode. Moreover, the second mode exhibits the single node with opposite deflections, while the third mode is marked by two nodes and higher curvature as seen in figure 18. Minor asymmetry in mode shapes is found due to different stiffnesses at both ends of the beam.

5.8.1 Comparative Discussion of Transverse Vibration Results

Based on the above analysis of the natural frequencies, it can be observed that the impact of the attached mass at the centre of the beam depends on the deformation of the centre point during the modal displacement. In the first mode of vibration, it can be observed that there is a drastic reduction in the natural frequency because of the behavior of the first bending mode, where the displacement is maximum at the centre position; hence, the impact of the attached mass is highly significant. In the second mode of vibration, the impact of the attached mass is insignificant because of the fact that the second mode of vibration is antisymmetric in nature, meaning that it has nodes at the middle part of the beam.

Table 5. Comparison of transverse natural frequencies with and without central lumped mass

Mode	Without Mass (Hz)	With Mass (Hz)	Change (%)
1	82.28	39.56	-51.92
2	247.59	236.03	-4.67
3	502.59	457.96	-8.88

CHAPTER 6. Conclusion & Recommendations

6.1 Conclusion

This research was thus successful in meeting the objective of investigating the vibration behavior of beams under elastic support with concentrated mass on the mid-span. It was possible to establish the formulation of the governing differential equation for both longitudinal and transverse vibrations of the beam by taking into consideration the elastic supports and concentrated mass through the application of the Hamilton principle.

Solutions for natural frequencies have been obtained satisfactorily in cases when the spring system was symmetric as well as asymmetric, considering the presence of lumped masses at centre of beam. From the data thus obtained, it can be concluded that natural frequencies increase with an increase in mode numbers for all cases and that longitudinal frequencies are much higher than the transverse frequencies as longitudinal frequencies are relatively stiffer. In case there are lumped masses, natural frequencies tend to decrease depending on mode numbers; however, only those cases with greater displacement at the centre get affected.

ANSYS finite element analyses agreed well with the frequencies and modes obtained analytically, thus verifying the proposed mathematical formulations. Small errors occurred in higher modes due to discretization and numerical approximations. In general, it can be concluded that elastic supports, asymmetric supports, and midpoint mass have an important effect on the dynamic behavior of beams. The results will prove beneficial for the design of spring-supported machinery and structures, such as machine members, shafts, flexible supports, mounted mechanisms, and light structural members.

6.2 Recommendations

In light of the current investigation, further work can explore incorporating the damping effect, nonlinearity of the spring force, load variation with time, and the presence of moving mass into the model.

- The use of Timoshenko beam theory may also be adopted to include shear deformation and rotary inertia for thick or short beams.
- Experimental validation using laboratory modal testing is strongly recommended to further confirm the analytical and numerical findings.

- Additional studies may investigate multiple lumped masses, distributed attachments, variable cross-sections, composite materials, crack effects, thermal loading, and uncertainty in spring stiffness parameters.
- Optimization techniques can also be applied to determine ideal spring constants and mass locations for vibration suppression.
- Furthermore, transient, forced, and harmonic response analyses may be carried out to evaluate resonance behavior under real operating conditions. These improvements would enhance the practical applicability of the developed model in advanced structural and mechanical design.

7. References

Abbas, L. K., Chen, D., Wang, G., & Rui, X. (2016). *Transfer matrix method of linear multibody systems for free vibration analysis of beam carrying elastically mounted point masses*. In Proceedings of the 5th International Conference on Mechanical Engineering, Materials and Energy (5th ICMEME2016) (pp. 20–24). Atlantis Press. https://doi.org/10.2991/icmeme-16.2016.4

Banerjee, J. R. (2012). Free vibration of beams carrying spring-mass systems—A dynamic stiffness approach. *Computers & Structures*, 104–105, 21–26. https://doi.org/10.1016/j.compstruc.2012.02.020

Chen, Y. (1963). On the vibration of beams or rods carrying a concentrated mass. *Journal of Applied Mechanics*, *30*(2), 310–311. https://doi.org/10.1115/1.3636537

Goel, R. P. (1976). Free vibrations of a beam-mass system with elastically restrained ends. *Journal of Sound and Vibration*, *47*(1), 9–14.

Hozhabrossadati, S. M., Aftabi Sani, A., & Mofid, M. (2015). Vibration of beam with elastically restrained ends and rotational spring-lumped rotary inertia system at mid-span. *International Journal of Structural Stability and Dynamics*, *15*(1), 1450040. https://doi.org/10.1142/S0219455414500400

Kukla, S. (1994). Free vibrations of axially loaded beams with concentrated masses and intermediate elastic supports. *Journal of Sound and Vibration*, *172*(4), 449–458. https://doi.org/10.1006/jsvi.1994.1188

Kumar, S. V., Sarkar, A., & Padmanabhan, C. (2019). Free vibration of spring-mounted beams. *Journal of Physics: Conference Series*, *1264*(1), 012026. https://doi.org/10.1088/1742-6596/1264/1/012026

Laura, P. A. A., Filipich, C. P., & Cortínez, V. H. (1987). Vibrations of beams and plates carrying concentrated masses. *Journal of Sound and Vibration*, *117*(3), 459–465. https://doi.org/10.1016/S0022-460X(87)80065-2

Lee, J. W. (2023). Free vibration analysis of elastically restrained tapered beams with concentrated mass and axial force. *Applied Sciences*, *13*(19), 10742. https://doi.org/10.3390/app131910742

Liu, W.-H., Wu, J.-R., & Huang, C.-C. (1988). Free vibration of beams with elastically restrained edges and intermediate concentrated masses. *Journal of Sound and Vibration, 122*(2), 193–207.

Xiao, H., Sheng, M., Liu, Z., & Wei, Z. (2013). The study on free vibration of elastically restrained beams carrying various types of attachments with arbitrary spatial distributions. *Shock and Vibration*, *20*(3), 369–383. https://doi.org/10.1155/2013/983451

Yayli, M. Ö., Aras, M., & Aksoy, S. (2014). An efficient analytical method for vibration analysis of a beam on elastic foundation with elastically restrained ends. *Shock and Vibration*, 2014, Article 159213. https://doi.org/10.1155/2014/159213

APPENDICES

APPENDIX 1. Analytical Solution for Longitudinal Vibration of the Spring-supported Beam without Lumped Mass

1. Problem Statement

A uniform rod undergoing axial (longitudinal) vibration is considered. The rod is supported by linear springs at both ends without considering center lumped mass.

The physical parameters are:

$$\mathrm{L} = 0.5\ \mathrm{m}$$

$$\mathrm{E} = 6.89 \times 10^{10}\ \mathrm{Pa}$$

$$\rho = 2.8 \times 10^{3}\ \mathrm{kg/m^3}$$

$$\mathrm{A} = 2 \times 10^{-4}\ \mathrm{m^2}$$

$$\mathrm{k_{LH}} = \mathrm{k_{RH}} = 10^{7}\ \mathrm{N/m}$$

Let the axial displacement of the rod be denoted by

$$\mathrm{u}(\mathrm{x}, \mathrm{t}).$$

The governing partial differential equation is

$$\rho \mathrm{A} \frac{\partial^2 \mathrm{u}}{\partial \mathrm{t}^2} = \frac{\partial}{\partial \mathrm{x}} \left(\mathrm{EA} \frac{\partial \mathrm{u}}{\partial \mathrm{x}} \right).$$

Since E and A are constant,

$$\rho \mathrm{A} \frac{\partial^2 \mathrm{u}}{\partial \mathrm{t}^2} = \mathrm{EA} \frac{\partial^2 \mathrm{u}}{\partial \mathrm{x}^2}.$$

The spring-supported boundary conditions are

$$\mathrm{EAU}'(0) - \mathrm{k_{LH}U}(0) = 0$$

and

$$\mathrm{EAU}'^{(\mathrm{L})} + \mathrm{k_{RH}U}(\mathrm{L}) = 0.$$

2. Separation of Variables

Assume the displacement field in separable form:

$$u(x,t) = U(x)q(t).$$

Substituting this into the governing equation gives

$$\rho A\, U(x)\ddot{q}(t) = EA\, U''(x)q(t).$$

Dividing by $EAU(x)q(t)$,

$$\frac{\rho}{E}\frac{\ddot{q}}{q} = \frac{U''}{U}.$$

Because the left-hand side depends only on t and the right-hand side depends only on x, each side must be equal to a constant. Let the separation constant be $-\lambda^2$. Therefore,

$$\frac{\ddot{q}}{q} = -\omega^2$$

and

$$\frac{U''}{U} = -\lambda^2.$$

Hence,

$$\ddot{q} + \omega^2 q = 0$$

and

$$U'' + \lambda^2 U = 0.$$

The wave speed is

$$c = \sqrt{\frac{E}{\rho}}.$$

Using,

$$c = \sqrt{\frac{6.89 \times 10^{10}}{2.8 \times 10^{3}}} = 4960.56 \text{ m/s}.$$

Therefore,

$$\omega = c\lambda.$$

3. General Spatial Solution

The spatial differential equation is

$$U'' + \lambda^2 U = 0.$$

Its general solution is

$$U(x) = A\cos(\lambda x) + B\sin(\lambda x).$$

Differentiating with respect to x,

$$U'^{(x)} = -A\lambda\sin(\lambda x) + B\lambda\cos(\lambda x).$$

4. Application of the Boundary Condition at $x = 0$

At $x = 0$,

$$U(0) = A$$

and

$$U'(0) = B\lambda.$$

Substitute these into the left-end boundary condition

$$EAU'(0) - k_{LH}U(0) = 0.$$

Then,

$$EA(B\lambda) - k_{LH}A = 0.$$

So,

$$EA\,B\lambda = k_{LH}A.$$

Hence,

$$B = \frac{k_{LH}}{EA\lambda}A.$$

Now compute the quantity EA:

$$EA = (6.89 \times 10^{10})(2 \times 10^{-4}) = 1.378 \times 10^{7}\ \text{N}.$$

Therefore,

$$B = \frac{10^7}{(1.378 \times 10^7)\lambda}A.$$

5. Application of the Boundary Condition at $x = L$

At $x = L$,

$$U(L) = A\cos(\lambda L) + B\sin(\lambda L)$$

and

$$U'(L) = -A\lambda\sin(\lambda L) + B\lambda\cos(\lambda L).$$

Substitute these into the right-end boundary condition

$$EAU'(L) + k_{RH}U(L) = 0.$$

This gives

$$EA[-A\lambda\sin(\lambda L) + B\lambda\cos(\lambda L)] + k_{RH}[A\cos(\lambda L) + B\sin(\lambda L)] = 0.$$

Now replace B using

$$B = \frac{k_{LH}}{EA\lambda}A.$$

Then,

$$EA\left[-A\lambda\sin(\lambda L) + \frac{k_{LH}}{EA\lambda}A \cdot \lambda\cos(\lambda L)\right] + k_{RH}\left[A\cos(\lambda L) + \frac{k_{LH}}{EA\lambda}A\sin(\lambda L)\right] = 0.$$

Simplifying,

$$EA[-A\lambda\sin(\lambda L)] + k_{LH}A\cos(\lambda L) + k_{RH}A\cos(\lambda L) + \frac{k_{LH}k_{RH}}{EA\lambda}A\sin(\lambda L) = 0.$$

Factoring out A:

$$A\left[-EA\lambda\sin(\lambda L) + (k_{LH} + k_{RH})\cos(\lambda L) + \frac{k_{LH}k_{RH}}{EA\lambda}\sin(\lambda L)\right] = 0.$$

For a nontrivial solution, $A \neq 0$. Therefore,

$$-EA\lambda\sin(\lambda L) + (k_{LH} + k_{RH})\cos(\lambda L) + \frac{k_{LH}k_{RH}}{EA\lambda}\sin(\lambda L) = 0.$$

Rearranging,

$$(k_{LH} + k_{RH})\cos(\lambda L) = \left(EA\lambda - \frac{k_{LH}k_{RH}}{EA\lambda}\right)\sin(\lambda L).$$

Dividing by $\cos(\lambda L)$ and by the coefficient on the right,

$$\tan(\lambda L) = \frac{(EA\lambda)(k_{LH} + k_{RH})}{(EA\lambda)^2 - k_{LH}k_{RH}}.$$

Since

$$k_{LH} = k_{RH} = k = 10^7 \text{ N/m},$$

the characteristic equation becomes

$$\tan(\lambda L) = \frac{2k(EA)\lambda}{(EA\lambda)^2 - k^2}.$$

With $L = 0.5$ m,

$$\tan(0.5\lambda) = \frac{2k(EA)\lambda}{(EA\lambda)^2 - k^2}.$$

Define

$$F(\lambda) = \tan(0.5\lambda) - \frac{2k(EA)\lambda}{(EA\lambda)^2 - k^2}.$$

The admissible eigenvalues are obtained from

$$F(\lambda) = 0.$$

6. Root Selection and Eigenvalues

The first three numerical roots approximately as

$$0.725689, \quad 1.653910, \quad 6.713866.$$

Those roots produced the frequencies

$$572.93 \text{ Hz}, \quad 1305.76 \text{ Hz}, \quad 5300.58 \text{ Hz}.$$

However, the supplied revised derivation states that the first low root is discarded as it gives a linear mode shape plot and the next admissible roots are selected. This discarded low root is also verified through ANSYS as the mass participation in the low root is seen significantly low. So that the analytical sequence matches the ANSYS mode sequence.

Therefore, the revised eigenvalues are taken as

$$\lambda_1 = 1.653911 \text{ m}^{-1}$$

$$\lambda_2 = 6.713945 \text{ m}^{-1}$$

and

$$\lambda_3 = 12.793574 \text{ m}^{-1}.$$

7. Natural Frequencies F_1, F_2 and F_3

The natural frequency is

$$\omega_n = c\lambda_n,$$

and the corresponding natural frequency in hertz is

$$F_n = \frac{\omega_n}{2\pi} = \frac{c\lambda_n}{2\pi}.$$

Using $c = 4960.56$ m/s:

Mode 1

$$\lambda_1 = 1.653911$$

$$F_1 = \frac{(4960.56)(1.653911)}{2\pi} = 1305.76 \text{ Hz.}$$

Mode 2

$$\lambda_2 = 6.713945$$

$$F_2 = \frac{(4960.56)(6.713945)}{2\pi} = 5300.64 \text{ Hz.}$$

Mode 3

$$\lambda_3 = 12.793574$$

$$F_3 = \frac{(4960.56)(12.793574)}{2\pi} = 10100.49 \text{ Hz.}$$

Hence, the revised analytical frequencies are

$$F_1 = 1305.76 \text{ Hz}, \qquad F_2 = 5300.64 \text{ Hz}, \qquad F_3 = 10100.49 \text{ Hz}.$$

8. Calculation of Constants A and B

Choosing

$$A_n = 1$$

for each mode.

From the left boundary condition,

$$B_n = \frac{k}{EA\lambda_n} A_n.$$

Using

$$EA = 1.378 \times 10^7, \qquad k = 10^7,$$

we obtain the constants for each mode as follows.

Mode 1

$$A_1 = 1$$

$$B_1 = \frac{10^7}{(1.378 \times 10^7)(1.653911)} = 0.438772.$$

Mode 2

$$A_2 = 1$$

$$B_2 = \frac{10^7}{(1.378 \times 10^7)(6.713945)} = 0.108087.$$

Mode 3

$$A_3 = 1$$

$$B_3 = \frac{10^7}{(1.378 \times 10^7)(12.793574)} = 0.056723.$$

9. Expressions for the Mode Shapes

The general mode-shape expression is

$$U_n(x) = A_n \cos(\lambda_n x) + B_n \sin(\lambda_n x).$$

Substituting the values of A_n, B_n and λ_n for each mode:

Mode 1

$$U_1(x) = \cos(1.653911x) + 0.438772\sin(1.653911x)$$

Mode 2

$$U_2(x) = \cos(6.713945x) + 0.108087\sin(6.713945x)$$

Mode 3

$$U_3(x) = \cos(12.793574x) + 0.056723\sin(12.793574x)$$

10. Normalization of the Mode Shapes

Each mode shape is normalized as

$$U_{n,\text{norm}}(x) = \frac{U_n(x)}{\max\limits_{0 \le x \le L} |U_n(x)|},$$

so that

$$-1 \leq U_{n,norm}(x) \leq 1.$$

These normalized forms are used to generate the final mode-shape curves.

11. Final Results Summary

Mode	$\boldsymbol{\lambda_n}$ **(m^{-1})**	$\boldsymbol{F_n}$ **(Hz)**	$\boldsymbol{A_n}$	$\boldsymbol{B_n}$
1	1.653911	1305.76	1	0.438772
2	6.713945	5300.64	1	0.108087
3	12.793574	10100.49	1	0.056723

Therefore, the final analytical mode shapes are

$$U_1(x) = \cos(1.653911x) + 0.438772\sin(1.653911x)$$

$$U_2(x) = \cos(6.713945x) + 0.108087\sin(6.713945x)$$

$$U_3(x) = \cos(12.793574x) + 0.056723\sin(12.793574x).$$

APPENDIX 2 Analytical Solution for Longitudinal Vibration of the Spring-Supported Beam with Central Lumped Mass

1. Problem statement

A uniform rod undergoing axial (longitudinal) vibration is considered. The rod is supported by linear springs at both ends and carries a concentrated disc mass at the centre, located at

$$a = \frac{L}{2}.$$

The axial displacement is denoted by $u(z, t)$. The rod parameters used in the supplied derivation are

Parameter	Value
Rod length, L	0.5 m
Young's modulus, E	6.89×10^{10} Pa
Density, ρ	2.8×10^{3} kg/m^{3}
Cross-sectional area, A	2×10^{-4} m^{2}
Left spring stiffness, k_L	1×10^{7} N/m
Right spring stiffness, k_R	1×10^{7} N/m

The axial rigidity is

$$EA = (6.89 \times 10^{10})(2 \times 10^{-4}) = 1.378 \times 10^{7} \text{ N}.$$

The axial wave speed is

$$c = \sqrt{\frac{E}{\rho}} = \sqrt{\frac{6.89 \times 10^{10}}{2.8 \times 10^{3}}} = 4960.56 \text{ m/s}.$$

The non-dimensional disc mass ratio is

$$\mu = \frac{M_d}{\rho A} = \frac{0.5}{(2800)(2 \times 10^{-4})} = 0.892857.$$

The spring-supported boundary conditions are

$$EAU'(0) - k_L U(0) = 0,$$

$$EAU'^{(L)} + k_R U(L) = 0.$$

2. Governing equation and separation of variables

For a uniform rod with a concentrated disc mass at $z = a$, the governing equation can be written in delta-function form as

$$[\rho A + M_d\,\delta(z-a)]\,\ddot{u}(z,t) - EA\,u_{zz}(z,t) = 0.$$

Assume a separable solution of the form

$$u(z,t) = U(z)q(t).$$

Substituting into the governing equation gives

$$[\rho A + M_d\,\delta(z-a)]U(z)\ddot{q}(t) - EAU''(z)q(t) = 0.$$

Dividing by $U(z)q(t)$ for nontrivial motion,

$$[\rho A + M_d\,\delta(z-a)]\frac{\ddot{q}}{q} = EA\frac{U''}{U}.$$

Set the separation constant equal to $-\omega^2$. Then the time equation becomes

$$\ddot{q} + \omega^2 q = 0,$$

and, away from $z = a$, the spatial equation becomes

$$EAU'' + \rho A\omega^2 U = 0.$$

Dividing by EA,

$$U'' + \lambda^2 U = 0,$$

where

$$\lambda^2 = \frac{\rho}{E}\omega^2, \qquad \omega = c\lambda, \qquad c = \sqrt{\frac{E}{\rho}}.$$

Therefore, the smooth solution away from the disc is

$$U(z) = A\cos(\lambda z) + B\sin(\lambda z).$$

3. Global mode-shape formulation using the Heaviside function

To avoid a piecewise expression, we define the global mode shape using the Heaviside step function $H(z-a)$ as

$$U(z) = A\cos(\lambda z) + B\sin(\lambda z) + C\,H(z-a)\sin\big(\lambda(z-a)\big).$$

This representation is convenient because

- it remains continuous at $z = a$,
- it automatically introduces the slope jump at the disc location, and

The derivative is

$$U'^{(z)} = -A\lambda\sin(\lambda z) + B\lambda\cos(\lambda z) + C\,H(z-a)\lambda\cos\big(\lambda(z-a)\big).$$

4. Jump condition at the disc location

Integrating the governing equation over a small interval around $z = a$. The disc (Lump Mass) produces a jump in axial slope:

$$EA[U'(a^+) - U'(a^-)] + \omega^2 M_d U(a) = 0.$$

Using $\omega = c\lambda$ and $c^2 = E/\rho$,

$$U'(a^+) - U'(a^-) = -\frac{M_d}{\rho A}\lambda^2 U(a) = -\mu\lambda^2 U(a).$$

From the global Heaviside term,

$$U'(a^+) - U'(a^-) = C\lambda.$$

Hence,

$$C\lambda = -\mu\lambda^2 U(a),$$

so that

$$C = -\mu\lambda U(a).$$

Now

$$U(a) = A\cos(\lambda a) + B\sin(\lambda a).$$

Therefore,

$$C = -\mu\lambda[A\cos(\lambda a) + B\sin(\lambda a)].$$

Substituting this into the global form, the final non-piecewise global mode shape becomes

$$U(z) = A\cos(\lambda z) + B\sin(\lambda z) - \mu\lambda[A\cos(\lambda a) + B\sin(\lambda a)]H(z-a)\sin\big(\lambda(z-a)\big).$$

This is the required global mode-shape expression.

5. Application of boundary conditions

5.1 Boundary condition at $z = 0$

Since $0 < \mathrm{a}$, the Heaviside term does not appear at $\mathrm{z} = 0$. Therefore,

$$\mathrm{U}(0) = \mathrm{A},$$

and

$$\mathrm{U}'(0) = \mathrm{B}\lambda.$$

Substituting into the left boundary condition,

$$\mathrm{EAU}'(0) - \mathrm{k_L U}(0) = 0,$$

we obtain

$$\mathrm{EA}(\mathrm{B}\lambda) - \mathrm{k_L A} = 0.$$

Hence,

$$\mathrm{B} = \frac{\mathrm{k_L}}{\mathrm{EA}\lambda}\mathrm{A}.$$

5.2 Evaluate $\mathrm{U}(\mathrm{a})$ in terms of A

Using

$$\mathrm{B} = \frac{\mathrm{k_L}}{\mathrm{EA}\lambda}\mathrm{A},$$

we get

$$\mathrm{U}(\mathrm{a}) = \mathrm{A}\cos(\lambda\mathrm{a}) + \frac{\mathrm{k_L}}{\mathrm{EA}\lambda}\mathrm{A}\sin(\lambda\mathrm{a}).$$

Factor out A:

$$\mathrm{U}(\mathrm{a}) = \mathrm{A}\left[\cos(\lambda\mathrm{a}) + \frac{\mathrm{k_L}}{\mathrm{EA}\lambda}\sin(\lambda\mathrm{a})\right].$$

Define

$$\mathrm{S}(\lambda) = \cos(\lambda\mathrm{a}) + \frac{\mathrm{k_L}}{\mathrm{EA}\lambda}\sin(\lambda\mathrm{a}).$$

Then

$$U(a) = AS(\lambda),$$

and therefore

$$C = -\mu\lambda AS(\lambda).$$

5.3 Boundary condition at $z = L$

For $L > a$, the Heaviside term is active, so $H(L - a) = 1$. The displacement at $z = L$ is

$$U(L) = A\cos(\lambda L) + B\sin(\lambda L) + C\sin\big(\lambda(L - a)\big),$$

and the derivative at $z = L$ is

$$U'(L) = -A\lambda\sin(\lambda L) + B\lambda\cos(\lambda L) + C\lambda\cos\big(\lambda(L - a)\big).$$

Substitute these into the right boundary condition

$$EAU'(L) + k_R U(L) = 0.$$

This gives

$$EA\big[-A\lambda\sin(\lambda L) + B\lambda\cos(\lambda L) + C\lambda\cos\big(\lambda(L - a)\big)\big]$$
$$+ k_R\big[A\cos(\lambda L) + B\sin(\lambda L) + C\sin\big(\lambda(L - a)\big)\big] = 0.$$

Substitute

$$B = \frac{k_L}{EA\lambda}A, \qquad C = -\mu\lambda AS(\lambda).$$

After collecting terms and factoring out A, the characteristic equation in λ becomes

$$-EA\lambda\sin(\lambda L) + (k_L + k_R)\cos(\lambda L) + \frac{k_L k_R}{EA\lambda}\sin(\lambda L)$$
$$- \mu S(\lambda)\big[EA\lambda^2\cos\big(\lambda(L - a)\big) + k_R\lambda\sin\big(\lambda(L - a)\big)\big] = 0.$$

This transcendental equation is solved numerically.

6. Derivation of eigenvalues λ_1, λ_2, and λ_3

For the present system,

$$L = 0.5\text{ m}, \qquad a = 0.25\text{ m}, \qquad EA = 1.378 \times 10^7\text{ N},$$

$$k_L = k_R = 10^7\text{ N/m}, \qquad \mu = 0.892857.$$

The roots are obtained numerically from the characteristic equation.

6.1 First eigenvalue

The first admissible root gives

$$\lambda_1 = 0.962121 \text{ m}^{-1}.$$

The corresponding natural circular frequency is

$$\omega_1 = c\lambda_1 = (4960.56)(0.962121) = 4773.69 \text{ rad/s}.$$

Hence the natural frequency is

$$F_1 = \frac{\omega_1}{2\pi} = \frac{(4960.56)(0.962121)}{2\pi} = 759.59 \text{ Hz}.$$

6.2 Second eigenvalue

The next admissible root gives

$$\lambda_2 = 6.713866 \text{ m}^{-1}.$$

Therefore,

$$\omega_2 = c\lambda_2 = (4960.56)(6.713866) = 33303.93 \text{ rad/s},$$

and

$$F_2 = \frac{\omega_2}{2\pi} = \frac{(4960.56)(6.713866)}{2\pi} = 5300.58 \text{ Hz}.$$

6.3 Third eigenvalue

The next admissible root gives

$$\lambda_3 = 7.777092 \text{ m}^{-1}.$$

Therefore,

$$\omega_3 = c\lambda_3 = (4960.56)(7.777092) = 38578.43 \text{ rad/s},$$

and

$$F_3 = \frac{\omega_3}{2\pi} = \frac{(4960.56)(7.777092)}{2\pi} = 6139.99 \text{ Hz}.$$

7. Calculation of constants for each mode

For scaling

$$A_n = 1 \qquad (n = 1,2,3).$$

Then

$$B_n = \frac{k_L}{EA\lambda_n} A_n,$$

and the disc-induced Heaviside coefficient is

$$C_n = -\mu\lambda_n U_n(a),$$

where

$$U_n(a) = A_n \cos(\lambda_n a) + B_n \sin(\lambda_n a).$$

7.1 Mode 1

For $\lambda_1 = 0.962121$ and $A_1 = 1$,

$$B_1 = \frac{10^7}{(1.378 \times 10^7)(0.962121)} = 0.754260.$$

At the disc location,

$$U_1(a) = \cos(0.962121 \times 0.25) + 0.754260 \sin(0.962121 \times 0.25) = 1.150890.$$

Hence,

$$C_1 = -\mu\lambda_1 U_1(a) = -(0.892857)(0.962121)(1.150890) = -0.988657.$$

Therefore, the first mode constants are

$$A_1 = 1, \qquad B_1 = 0.754260, \qquad C_1 = -0.988657.$$

7.2 Mode 2

For $\lambda_2 = 6.713866$ and $A_2 = 1$,

$$B_2 = \frac{10^7}{(1.378 \times 10^7)(6.713866)} = 0.108088.$$

At the disc location,

$$U_2(a) = \cos(6.713866 \times 0.25) + 0.108088 \sin(6.713866 \times 0.25) \approx 0.$$

Hence,

$$C_2 = -\mu\lambda_2 U_2(a) \approx 0.$$

Therefore, the second mode constants are

$$A_2 = 1, \qquad B_2 = 0.108088, \qquad C_2 \approx 0.$$

7.3 Mode 3

For $\lambda_3 = 7.777092$ and $A_3 = 1$,

$$B_3 = \frac{10^7}{(1.378 \times 10^7)(7.777092)} = 0.093311.$$

At the disc location,

$$U_3(a) = \cos(7.777092 \times 0.25) + 0.093311\sin(7.777092 \times 0.25) = -0.277976.$$

Hence,

$$C_3 = -\mu\lambda_3 U_3(a) = -(0.892857)(7.777092)(-0.277976) = 1.930219.$$

Therefore, the third mode constants are

$$A_3 = 1, \qquad B_3 = 0.093311, \qquad C_3 = 1.930219.$$

8. Expressions for the three global mode shapes

Using $a = L/2 = 0.25$ m and the computed constants, the three global mode shapes are

8.1 Mode 1

$$U_1(z) = \cos(0.962121z) + 0.754260\sin(0.962121z) - 0.988657\, H(z - 0.25)\sin\big(0.962121(z - 0.25)\big).$$

8.2 Mode 2

$$U_2(z) = \cos(6.713866z) + 0.108088\sin(6.713866z) + 0 \cdot H(z - 0.25)\sin\big(6.713866(z - 0.25)\big).$$

Since $C_2 \approx 0$, this can be written more compactly as

$$U_2(z) = \cos(6.713866z) + 0.108088\sin(6.713866z).$$

8.3 Mode 3

$$U_3(z) = \cos(7.777092z) + 0.093311\sin(7.777092z) + 1.930219\, H(z - 0.25)\sin\big(7.777092(z - 0.25)\big).$$

9. Normalization

To plot the mode shapes in normalized form, use

$$U_{n,\mathrm{norm}}(z) = \frac{U_n(z)}{\max\limits_{0 \le z \le L} |U_n(z)|}.$$

This ensures that each normalized mode shape satisfies

$$-1 \leq U_{n,norm}(z) \leq 1.$$

10. Final presentation and summary of results

The final computed quantities are summarized below.

Mode	$\boldsymbol{\lambda_n}$ **(m^{-1})**	$\mathbf{F_n}$ **(Hz)**	$\mathbf{A_n}$	$\mathbf{B_n}$	$\mathbf{C_n}$
1	0.962121	759.59	1	0.754260	-0.988657
2	6.713866	5300.58	1	0.108088	≈ 0
3	7.777092	6139.99	1	0.093311	1.930219

APPENDIX 3. Analytical Solution for Transverse Vibration of the Spring-supported Beam without Lumped Mass

1. Problem statement

A uniform Euler-Bernoulli beam of length L undergoes free transverse vibration. Both beam ends are restrained by translational springs. Following the supplied derivation, the governing equation, the four boundary conditions, the characteristic equation, the 4×4 coefficient matrix, the Eigen valuesβ_1, β_2, β_3, the modal constants (A, B, C, D), and the normalized mode-shape plots are prepared:

Parameter	Value
Length, L	0.5 m
Young's modulus, E	6.89×10^{10} Pa
Density, ρ	2.8×10^{3} kg/m^3
Area, A	2×10^{-4} m^2
Second moment of area, I	1.677×10^{-9} m^4
Left spring stiffness, k_{LV}	10^7 N/m
Right spring stiffness, k_{RV}	10^7 N/m

Hence,

$$EI = (6.89 \times 10^{10})(1.677 \times 10^{-9}) = 115.5453 \text{ N} \cdot \text{m}^2$$

and

$$\rho A = (2.8 \times 10^{3})(2 \times 10^{-4}) = 0.56 \text{ kg/m}.$$

2. Governing Differential Equation and Boundary Conditions

The governing transverse bending PDE is

$$\rho A\, \ddot{w}(x,t) + EI\, w_{xxxx}(x,t) = 0.$$

The four boundary conditions used are as follows.

At $\mathbf{x = 0}$

Boundary condition 1: zero bending moment

$$\mathrm{EI}\, w_{xx}(0,t) = 0.$$

Boundary condition 2: shear-spring relation

$$\mathrm{EI}\, w_{xxx}(0,t) + k_{LV}\, w(0,t) = 0.$$

At x = L

Boundary condition 3: zero bending moment

$$\mathrm{EI}\, w_{xx}(L,t) = 0.$$

Boundary condition 4: shear-spring relation

$$\mathrm{EI}\, w_{xxx}(L,t) - k_{RV}\, w(L,t) = 0.$$

3. Separation of Variables

Assume the separable solution

$$w(x,t) = W(x)\, q(t).$$

Substituting into the governing PDE gives

$$\rho A\, W\, \ddot{q} + \mathrm{EI}\, W^{(4)} q = 0.$$

Dividing by Wq gives

$$\rho A\, \frac{\ddot{q}}{q} + \mathrm{EI}\, \frac{W^{(4)}}{W} = 0.$$

Rearranging,

$$\frac{\ddot{q}}{q} = -\frac{\mathrm{EI}}{\rho A}\frac{W^{(4)}}{W}.$$

Set both sides equal to the separation constant $-\omega^2$. Then

$$\ddot{q} + \omega^2 q = 0$$

and

$$W^{(4)} - \beta^4 W = 0,$$

where

$$\beta^4 = \frac{\rho A\,\omega^2}{EI} \qquad \Rightarrow \qquad \omega = \beta^2\sqrt{\frac{EI}{\rho A}}.$$

Using the numerical values,

$$\sqrt{\frac{EI}{\rho A}} = \sqrt{\frac{115.5453}{0.56}} = 14.36422267.$$

4. General Solution of the Spatial ODE

For

$$W^{(4)} - \beta^4 W = 0,$$

the standard spatial solution is

$$W(x) = A\cosh(\beta x) + B\sinh(\beta x) + C\cos(\beta x) + D\sin(\beta x).$$

Its derivatives are

$$W'(x) = \beta[A\sinh(\beta x) + B\cosh(\beta x) - C\sin(\beta x) + D\cos(\beta x)],$$

$$W''(x) = \beta^2[A\cosh(\beta x) + B\sinh(\beta x) - C\cos(\beta x) - D\sin(\beta x)],$$

$$W'''(x) = \beta^3[A\sinh(\beta x) + B\cosh(\beta x) + C\sin(\beta x) - D\cos(\beta x)].$$

5. Application of All Four Boundary Conditions

5.1 Apply BC1: $EI\,W''(0) = 0$

At $x = 0$,

$$\cosh 0 = 1, \qquad \sinh 0 = 0, \qquad \cos 0 = 1, \qquad \sin 0 = 0.$$

Therefore,

$$W''(0) = \beta^2(A - C).$$

Thus,

$$EI\beta^2(A - C) = 0$$

which gives

$$A - C = 0 \qquad \Rightarrow \qquad A = C.$$

5.2 Apply BC2: $EI\,W'''(0) + k_{LV}W(0) = 0$

At $x = 0$,

$$W'''(0) = \beta^3(B - D), \qquad W(0) = A + C.$$

Substituting into BC2,

$$EI\beta^3(B - D) + k_{LV}(A + C) = 0.$$

Expanding into the constants gives

$$k_{LV}A + EI\beta^3 B + k_{LV}C - EI\beta^3 D = 0.$$

5.3 Apply BC3: $EI\,W''(L) = 0$

Let

$$\lambda = \beta L.$$

Then

$$W''(L) = \beta^2[A\cosh\lambda + B\sinh\lambda - C\cos\lambda - D\sin\lambda].$$

Hence,

$$A\cosh\lambda + B\sinh\lambda - C\cos\lambda - D\sin\lambda = 0.$$

5.4 Apply BC4: $EI\,W'''(L) - k_{RV}W(L) = 0$

First write

$$W'''(L) = \beta^3[A\sinh\lambda + B\cosh\lambda + C\sin\lambda - D\cos\lambda],$$

and

$$W(L) = A\cosh\lambda + B\sinh\lambda + C\cos\lambda + D\sin\lambda.$$

Substituting into BC4 gives

$$EI\beta^3[A\sinh\lambda + B\cosh\lambda + C\sin\lambda - D\cos\lambda] - k_{RV}[A\cosh\lambda + B\sinh\lambda + C\cos\lambda + D\sin\lambda] = 0.$$

Collecting coefficients of A, B, C, and D,

$$(EI\beta^3\sinh\lambda - k_{RV}\cosh\lambda)A + (EI\beta^3\cosh\lambda - k_{RV}\sinh\lambda)B$$

$$+(EI\beta^3\sin\lambda - k_{RV}\cos\lambda)C + (-EI\beta^3\cos\lambda - k_{RV}\sin\lambda)D = 0.$$

6. Formation of the 4×4 Matrix System

Collecting BC1 to BC4 together,

$$K(\beta)\begin{bmatrix} A \\ B \\ C \\ D \end{bmatrix} = \begin{bmatrix} 0 \\ 0 \\ 0 \\ 0 \end{bmatrix},$$

where

$$K(\beta) = \begin{bmatrix} 1 & 0 & -1 & 0 \\ k_{LV} & EI\beta^3 & k_{LV} & -EI\beta^3 \\ \cosh\lambda & \sinh\lambda & -\cos\lambda & -\sin\lambda \\ EI\beta^3\sinh\lambda - k_{RV}\cosh\lambda & EI\beta^3\cosh\lambda - k_{RV}\sinh\lambda & EI\beta^3\sin\lambda - k_{RV}\cos\lambda & -EI\beta^3\cos\lambda - k_{RV}\sin\lambda \end{bmatrix}$$

For a non-trivial solution,

$$\det[\mathrm{K}(\beta)] = 0.$$

This determinant equation is the frequency equation from which the eigenvalues β_1, β_2, and β_3 are obtained.

7. Derivation of the Eigenvalues β_1, β_2, and β_3

Using the supplied numerical values,

$$\mathrm{E} = 6.89 \times 10^{10}, \qquad \rho = 2.8 \times 10^{3}, \qquad \mathrm{L} = 0.5, \qquad \mathrm{A} = 2 \times 10^{-4}, \qquad \mathrm{I} = 1.677 \times 10^{-9},$$

$$\mathrm{EI} = 115.5453\ \mathrm{N \cdot m^2}, \qquad \rho\mathrm{A} = 0.56\ \mathrm{kg/m}, \qquad \mathrm{k_{LV}} = \mathrm{k_{RV}} = 10^7\ \mathrm{N/m}.$$

Solving

$$\det[\mathrm{K}(\beta)] = 0$$

produces the first three eigenvalues reported in the supplied PDF:

$$\beta_1 = 6.277461255\ \mathrm{rad/m}$$

$$\beta_2 = 12.520493156\ \mathrm{rad/m}$$

$$\beta_3 = 18.692778432\ \mathrm{rad/m}.$$

8. Natural Frequencies ω_n and f_n

The natural circular frequencies are computed from

$$\omega_n = \beta_n^2\sqrt{\frac{\mathrm{EI}}{\rho\mathrm{A}}},$$

and the natural frequencies in hertz are

$$f_n = \frac{\omega_n}{2\pi}.$$

Since

$$\sqrt{\frac{EI}{\rho A}} = 14.36422267,$$

the first three natural frequencies are obtained one by one as follows.

Mode 1

$$\omega_1 = (6.277461255)^2(14.36422267) = 566.0440 \text{ rad/s}$$

$$f_1 = \frac{566.0440}{2\pi} = 90.0887 \text{ Hz.}$$

Mode 2

$$\omega_2 = (12.520493156)^2(14.36422267) = 2251.7750 \text{ rad/s}$$

$$f_2 = \frac{2251.7750}{2\pi} = 358.3811 \text{ Hz.}$$

Mode 3

$$\omega_3 = (18.692778432)^2(14.36422267) = 5019.1462 \text{ rad/s}$$

$$f_3 = \frac{5019.1462}{2\pi} = 798.8219 \text{ Hz.}$$

9. Calculation of the Constants A, B, C, and D

For scaling,

$$A = 1.$$

From BC1,

$$A = C \qquad \Rightarrow \qquad C = 1.$$

Thus only B and D remain to be determined for each mode.

9.1 Relation between B and D from BC2

From BC2,

$$EI\beta^3(B - D) + k_{LV}(A + C) = 0.$$

Using $A = C = 1$,

$$EI\beta^3(B - D) + 2k_{LV} = 0.$$

Hence,

$$B - D = -\frac{2k_{LV}}{EI\beta^3}.$$

Define

$$\Delta(\beta) = \frac{2k_{LV}}{EI\beta^3}.$$

Then

$$B - D = -\Delta(\beta) \qquad \Rightarrow \qquad D = B + \Delta(\beta).$$

9.2 Solve for B from BC3

BC3 is

$$A\cosh\lambda + B\sinh\lambda - C\cos\lambda - D\sin\lambda = 0.$$

Substituting $A = C = 1$ and $D = B + \Delta(\beta)$,

$$\cosh\lambda + B\sinh\lambda - \cos\lambda - \big(B + \Delta(\beta)\big)\sin\lambda = 0.$$

Grouping the terms in B,

$$B(\sinh\lambda - \sin\lambda) + (\cosh\lambda - \cos\lambda) - \Delta(\beta)\sin\lambda = 0.$$

Therefore,

$$B = \frac{\cos\lambda - \cosh\lambda + \Delta(\beta)\sin\lambda}{\sinh\lambda - \sin\lambda}.$$

Once B is known,

$$D = B + \Delta(\beta).$$

Because β_n is already a root of $\det[K(\beta)] = 0$, BC4 is automatically satisfied by the corresponding constants.

10. Constants for the First Three Modes

Using $k_{LV} = k_{RV} = 10^7$ N/m and the eigenvalues obtained above, the constants are:

Mode 1: $\beta_1 = 6.277461255$

$$A_1 = 1, \qquad C_1 = 1, \qquad B_1 = -0.9169247470, \qquad D_1 = 698.8051713908.$$

Mode 2: $\boldsymbol{\beta_2 = 12.520493156}$

$$A_2 = 1, \qquad C_2 = 1, \qquad B_2 = -1.0038288653, \qquad D_2 = 87.1849655534.$$

Mode 3: $\boldsymbol{\beta_3 = 18.692778432}$

$$A_3 = 1, \qquad C_3 = 1, \qquad B_3 = -0.9998254552, \qquad D_3 = 25.5008007519.$$

11. Expressions of the Mode Shapes

The general mode-shape expression is

$$W_n(x) = A_n\cosh(\beta_n x) + B_n\sinh(\beta_n x) + C_n\cos(\beta_n x) + D_n\sin(\beta_n x).$$

Therefore, the first three transverse mode shapes are:

Mode 1

$$W_1(x) = \cosh(\beta_1 x) - 0.9169247470\sinh(\beta_1 x) + \cos(\beta_1 x) + 698.8051713908\sin(\beta_1 x).$$

Mode 2

$$W_2(x) = \cosh(\beta_2 x) - 1.0038288653\sinh(\beta_2 x) + \cos(\beta_2 x) + 87.1849655534\sin(\beta_2 x).$$

Mode 3

$$W_3(x) = \cosh(\beta_3 x) - 0.9998254552\sinh(\beta_3 x) + \cos(\beta_3 x) + 25.5008007519\sin(\beta_3 x).$$

12. Normalization of the Mode Shapes

Each mode shape is normalized by its maximum absolute value over the beam span:

$$W_{n,\text{norm}}(x) = \frac{W_n(x)}{\max\limits_{0\le x\le L}|W_n(x)|}.$$

Therefore,

$$-1 \le W_{n,\text{norm}}(x) \le 1.$$

13. Final Results Summary

Mode	**β_n (rad/m)**	**ω_n (rad/s)**	**f_n (Hz)**	**A_n**	**B_n**	**C_n**	**D_n**
1	6.2774612 55	566.0440	90.0887	1	-0.9169247 470	1	698.8051 713908
2	12.5204931 56	2251.7750	358.3811	1	-1.0038288 653	1	87.184965 5534
3	18.6927784 32	5019.1462	798.8219	1	-0.9998254 552	1	25.500800 7519

APPENDIX 4. Analytical Solution for Transverse Vibration of the Spring-supported Beam with Central Lumped Mass

1. Problem statement

We consider a uniform Euler-Bernoulli beam of total length

$$L = 0.5 \text{ m},$$

undergoing transverse vibration. The beam has flexural rigidity EI, distributed mass ρA, and equal transverse support springs at the two ends. A concentrated disc mass is attached at the beam centre.

The support stiffnesses are

$$k_{LV} = k_{RV} = 10^7 \text{ N/m}.$$

The governing equation is

$$\rho A\, w_{tt}(z,t) + EI\, w_{zzzz}(z,t) + m_d\, \delta\left(z - \frac{L}{2}\right) w_{tt}(z,t) = 0.$$

The end boundary conditions are

$$EI\, w_{zz}(0,t) = 0,$$

$$EI\, w_{zzz}(0,t) + k_{LV}\, w(0,t) = 0,$$

$$EI\, w_{zz}(L,t) = 0,$$

$$EI\, w_{zzz}(L,t) + k_{RV}\, w(L,t) = 0.$$

The centre conditions implied by the delta-mass term are

$$w^- = w^+, \qquad w_z^- = w_z^+, \qquad w_{zz}^- = w_{zz}^+,$$

and the shear jump condition at the centre is written as

$$EI[w_{zzz}^+ - w_{zzz}^-]_{z=L/2} = m_d\, w_{tt}\left(\frac{L}{2}, t\right).$$

Using the values,

$$E = 6.89 \times 10^{10} \text{ Pa}, \qquad \rho = 2.8 \times 10^3 \text{ kg/m}^3,$$

$$A = 2 \times 10^{-4} \text{ m}^2, \qquad I = 1.677 \times 10^{-9} \text{ m}^4,$$

$$EI = 115.5453 \text{ N m}^2, \qquad \rho A = 0.56 \text{ kg/m},$$

$$m_d = 0.5\ \text{kg}, \qquad l = \frac{L}{2} = 0.25\ \text{m}.$$

2. Derivation of Eigenvalues β_1, β_2 and β_3

2.1 Separation of variables

Assume separable solution of the form

$$w(z,t) = W(z)\, q(t).$$

Substituting into the governing equation away from the disc gives

$$\rho A\, W(z)\, \ddot{q}(t) + EI\, W^{(4)}(z)\, q(t) = 0.$$

Divide by Wq:

$$\frac{\ddot{q}}{q} = -\omega^2.$$

Hence the time equation becomes

$$\ddot{q} + \omega^2 q = 0,$$

and the spatial equation becomes

$$EI\, W^{(4)} - \rho A\, \omega^2 W = 0.$$

Define

$$\beta^4 = \frac{\rho A\, \omega^2}{EI}.$$

Then the spatial ordinary differential equation reduces to

$$W^{(4)} - \beta^4 W = 0.$$

3. General solution of the spatial equation

The standard closed-form solution of the spatial equation is

$$W(z) = A\cosh(\beta z) + B\sinh(\beta z) + C\cos(\beta z) + D\sin(\beta z).$$

Its derivatives are

$$W'(z) = \beta[A\sinh(\beta z) + B\cosh(\beta z) - C\sin(\beta z) + D\cos(\beta z)],$$

$$W''(z) = \beta^2[A\cosh(\beta z) + B\sinh(\beta z) - C\cos(\beta z) - D\sin(\beta z)],$$

$$W'''(z) = \beta^3[A\sinh(\beta z) + B\cosh(\beta z) + C\sin(\beta z) - D\cos(\beta z)].$$

4. Why the modified problem is not a direct full-beam 4×4 system?

For the beam without a centre disc, the four end boundary conditions are sufficient to produce a single 4×4 homogeneous system in the constants A, B, C and D over the full span.

For the present modified problem, the centre disc introduces a shear-force jump at $z = L/2$. Therefore, the exact full-beam description is not a direct one-span 4×4 system. Instead, the full-beam solution must be viewed as two span functions:

$$W_L(z) = A_1\cosh(\beta z) + B_1\sinh(\beta z) + C_1\cos(\beta z) + D_1\sin(\beta z), \qquad 0 \le z \le \frac{L}{2},$$

$$W_R(z) = A_2\cosh(\beta z) + B_2\sinh(\beta z) + C_2\cos(\beta z) + D_2\sin(\beta z), \qquad \frac{L}{2} \le z \le L.$$

Thus, the exact full-beam problem contains

- 4 end conditions, and
- 4 centre conditions,

which gives an 8×8 homogeneous system.

Because the beam, the centre mass, and the end springs are symmetric, the problem may be reduced to a half-beam formulation. It leads to separate symmetric and anti-symmetric families.

5. Symmetry reduction to the half-beam

Work only on the half-beam

$$0 \le z \le l, \qquad l = \frac{L}{2} = 0.25 \text{ m}.$$

Use the same spatial form

$$W(z) = A\cosh(\beta z) + B\sinh(\beta z) + C\cos(\beta z) + D\sin(\beta z).$$

At the left end $z = 0$, the boundary conditions are

$$EI\,W''(0) = 0,$$

$$EI\,W'''(0) + k_{LV}W(0) = 0.$$

At the centre $z = l$, the additional conditions depend on whether the mode is symmetric or anti-symmetric.

First two conditions at $\mathbf{z = 0}$

BC1

At $z = 0$,

$$W''(0) = \beta^2(A - C).$$

Applying $EI\,W''(0) = 0$ gives

$$EI\beta^2(A - C) = 0.$$

Hence

$$A - C = 0 \qquad \Rightarrow \qquad C = A.$$

BC2

At $z = 0$,

$$W'''(0) = \beta^3(B - D), \qquad W(0) = A + C.$$

Therefore,

$$EI\beta^3(B - D) + k_{LV}(A + C) = 0.$$

Using $C = A$,

$$EI\beta^3(B - D) + 2k_{LV}A = 0.$$

Thus,

$$B - D = -\frac{2k_{LV}}{EI\beta^3}A.$$

Define

$$\Delta(\beta) = \frac{2k_{LV}}{EI\beta^3}.$$

Then

$$D = B + \Delta(\beta)\,A.$$

6. Symmetric modes

6.1 Centre conditions for symmetric modes

For symmetric motion, the slope at the centre vanishes:

$$W'(l) = 0.$$

For the shear jump relation, symmetry implies that the shear on the right half is the mirror image of the shear on the left half. Substituting the harmonic time factor gives

$$2EI\,W'''(l) + m_d\omega^2\,W(l) = 0.$$

Therefore, the four homogeneous equations for the symmetric family are

$$A - C = 0,$$

$$k_{LV}A + EI\beta^3 B + k_{LV}C - EI\beta^3 D = 0,$$

$$A\sinh\lambda + B\cosh\lambda - C\sin\lambda + D\cos\lambda = 0,$$

$$\begin{aligned}(2EI\beta^3\sinh\lambda + m_d\omega^2\cosh\lambda)A + (2EI\beta^3\cosh\lambda + m_d\omega^2\sinh\lambda)B \\ + (2EI\beta^3\sin\lambda + m_d\omega^2\cos\lambda)C + (-2EI\beta^3\cos\lambda + m_d\omega^2\sin\lambda)D = 0,\end{aligned}$$

where

$$\lambda = \beta l.$$

6.2 Symmetric 4 × 4 matrix

The four equations can be written in matrix form as

$$K_s(\beta)\begin{bmatrix}A\\B\\C\\D\end{bmatrix} = \begin{bmatrix}0\\0\\0\\0\end{bmatrix},$$

with

$$K_s(\beta) = \begin{bmatrix} 1 & 0 & -1 & 0 \\ k_{LV} & EI\beta^3 & k_{LV} & -EI\beta^3 \\ \sinh\lambda & \cosh\lambda & -\sin\lambda & \cos\lambda \\ 2EI\beta^3\sinh\lambda + m_d\omega^2\cosh\lambda & 2EI\beta^3\cosh\lambda + m_d\omega^2\sinh\lambda & 2EI\beta^3\sin\lambda + m_d\omega^2\cos\lambda & -2EI\beta^3\cos\lambda + m_d\omega^2\sin\lambda \end{bmatrix}.$$

For a non-trivial solution, the determinant must vanish:

$$\det[K_s(\beta)] = 0.$$

This is the symmetric frequency equation.

7. Anti-symmetric modes

7.1 Centre conditions for anti-symmetric modes

For anti-symmetric modes, the centre displacement is zero and the curvature at the centre is zero:

$$W(l) = 0, \qquad W''(l) = 0.$$

Thus the four homogeneous equations become

$$A - C = 0,$$

$$k_{LV}A + EI\beta^3 B + k_{LV}C - EI\beta^3 D = 0,$$

$$A\cosh\lambda + B\sinh\lambda + C\cos\lambda + D\sin\lambda = 0,$$

$$A\cosh\lambda + B\sinh\lambda - C\cos\lambda - D\sin\lambda = 0.$$

7.2 Anti-symmetric 4×4 matrix

Hence

$$K_a(\beta)\begin{bmatrix} A \\ B \\ C \\ D \end{bmatrix} = \begin{bmatrix} 0 \\ 0 \\ 0 \\ 0 \end{bmatrix},$$

with

$$K_a(\beta) = \begin{bmatrix} 1 & 0 & -1 & 0 \\ k_{LV} & EI\beta^3 & k_{LV} & -EI\beta^3 \\ \cosh\lambda & \sinh\lambda & \cos\lambda & \sin\lambda \\ \cosh\lambda & \sinh\lambda & -\cos\lambda & -\sin\lambda \end{bmatrix}.$$

The anti-symmetric frequency equation is therefore

$$\det[K_a(\beta)] = 0.$$

8. Numerical roots and natural frequencies

Using

$$EI = 115.5453, \qquad \rho A = 0.56, \qquad l = 0.25, \qquad k_{LV} = 10^7, \qquad m_d = 0.5,$$

together with

$$\omega^2 = \beta^4 \frac{EI}{\rho A}, \qquad \omega = \beta^2 \sqrt{\frac{EI}{\rho A}}, \qquad f = \frac{\omega}{2\pi},$$

the determinant equations give the first three roots

$$\beta_1 = 4.284723969\ \mathrm{m}^{-1},$$

$$\beta_2 = 12.520493156\ \mathrm{m}^{-1},$$

$$\beta_3 = 16.096693800\ \mathrm{m}^{-1}.$$

Here

- β_1 is the first symmetric root of $\det[K_s(\beta)] = 0$,
- β_2 is the first anti-symmetric root of $\det[K_a(\beta)] = 0$,
- β_3 is the second symmetric root of $\det[K_s(\beta)] = 0$.

Also,

$$\sqrt{\frac{EI}{\rho A}} = 14.364222668.$$

Hence

$$\omega_1 = \beta_1^2\sqrt{\frac{EI}{\rho A}} = 263.710746 \text{ rad/s}, \qquad f_1 = 41.970869 \text{ Hz},$$

$$\omega_2 = \beta_2^2\sqrt{\frac{EI}{\rho A}} = 2251.775031 \text{ rad/s}, \qquad f_2 = 358.381127 \text{ Hz},$$

$$\omega_3 = \beta_3^2\sqrt{\frac{EI}{\rho A}} = 3721.821105 \text{ rad/s}, \qquad f_3 = 592.346226 \text{ Hz}.$$

9. Calculation of Constants A, B, C and D

Because the eigenvector system is homogeneous, one amplitude may be chosen arbitrarily. Following the usual mode-shape convention, we take

$$A = 1.$$

From $A - C = 0$, we obtain

$$C = 1.$$

The remaining constants are found from the centre and boundary relations.

Mode 1: first symmetric mode ($\boldsymbol{\beta_1 = 4.284723969}$)

For symmetric modes,

$$D = B + \Delta(\beta)A, \qquad \Delta(\beta) = \frac{2k_{LV}}{EI\beta^3}.$$

For $\beta = \beta_1$,

$$\Delta(\beta_1) = \frac{2k_{LV}}{EI\beta_1^3} = 2200.438141.$$

The centre slope condition $W'(l) = 0$ gives

$$A\sinh\lambda_1 + B\cosh\lambda_1 - C\sin\lambda_1 + D\cos\lambda_1 = 0,$$

where

$$\lambda_1 = \beta_1 l = 1.071180992.$$

Substituting $A = C = 1$ and $D = B + \Delta(\beta_1)$,

$$\sinh\lambda_1 + B\cosh\lambda_1 - \sin\lambda_1 + \big(B + \Delta(\beta_1)\big)\cos\lambda_1 = 0.$$

Collecting the terms in B gives

$$B(\cosh\lambda_1 + \cos\lambda_1) + \sinh\lambda_1 - \sin\lambda_1 + \Delta(\beta_1)\cos\lambda_1 = 0.$$

Hence

$$B_1 = -\frac{\sinh\lambda_1 - \sin\lambda_1 + \Delta(\beta_1)\cos\lambda_1}{\cosh\lambda_1 + \cos\lambda_1} = -499.863811.$$

Then

$$D_1 = B_1 + \Delta(\beta_1) = 1700.574330.$$

Therefore the first-mode constants are

$$A_1 = 1, \qquad B_1 = -499.863811, \qquad C_1 = 1, \qquad D_1 = 1700.574330.$$

Mode 2: first anti-symmetric mode ($\boldsymbol{\beta_2 = 12.520493156}$)

For the anti-symmetric family, the centre conditions are

$$W(l) = 0, \qquad W''(l) = 0.$$

Using $A = C = 1$, these become

$$\cosh\lambda_2 + B\sinh\lambda_2 + \cos\lambda_2 + D\sin\lambda_2 = 0,$$

$$\cosh\lambda_2 + B\sinh\lambda_2 - \cos\lambda_2 - D\sin\lambda_2 = 0,$$

with

$$\lambda_2 = \beta_2 l = 3.130123289.$$

Add and subtract the two equations. Then

$$2(\cosh\lambda_2 + B\sinh\lambda_2) = 0,$$

$$2(\cos\lambda_2 + D\sin\lambda_2) = 0.$$

Hence

$$B_2 = -\frac{\cosh\lambda_2}{\sinh\lambda_2} = -1.003829,$$

$$D_2 = -\frac{\cos\lambda_2}{\sin\lambda_2} = 87.184965.$$

The left-end boundary relation gives the same compatibility result because

$$D = B + \Delta(\beta), \qquad \Delta(\beta_2) = \frac{2k_{LV}}{EI\beta_2^3} = 88.188794,$$

and numerically

$$B_2 + \Delta(\beta_2) = 87.184966 \approx D_2.$$

Therefore the second-mode constants are

$$A_2 = 1, \qquad B_2 = -1.003829, \qquad C_2 = 1, \qquad D_2 = 87.184965.$$

Mode 3: second symmetric mode ($\boldsymbol{\beta_3 = 16.096693800}$)

Again,

$$A_3 = 1, \qquad C_3 = 1.$$

For $\beta = \beta_3$,

$$\Delta(\beta_3) = \frac{2k_{LV}}{EI\beta_3^3} = 41.501870, \qquad \lambda_3 = \beta_3 l = 4.024173450.$$

Using the same symmetric-mode reduction,

$$B_3 = -\frac{\sinh\lambda_3 - \sin\lambda_3 + \Delta(\beta_3)\cos\lambda_3}{\cosh\lambda_3 + \cos\lambda_3} = -0.086689,$$

and

$$D_3 = B_3 + \Delta(\beta_3) = 41.415181.$$

Therefore the third-mode constants are

$$A_3 = 1, \qquad B_3 = -0.086689, \qquad C_3 = 1, \qquad D_3 = 41.415181.$$

10. Expression of Mode Shapes

Define the half-beam function

$$\psi_n(z) = A_n\cosh(\beta_n z) + B_n\sinh(\beta_n z) + C_n\cos(\beta_n z) + D_n\sin(\beta_n z), \qquad 0 \le z \le l.$$

Then the full-beam mode shape is reconstructed as follows.

For the symmetric modes ($n = 1,3$),

$$W_n(z) = \psi_n(z)\, H(l - z) + \psi_n(L - z)\, H(z - l),$$

where $H(\cdot)$ is the Heaviside function.

For the anti-symmetric mode ($n = 2$),

$$W_2(z) = \psi_2(z)\, H(l - z) - \psi_2(L - z)\, H(z - l).$$

Mode shape equations with constants included

Mode 1

$$\psi_1(z) = \cosh(4.284723969z) - 499.863811\sinh(4.284723969z) + \cos(4.284723969z) + 1700.574330\sin(4.284723969z).$$

Hence

$$W_1(z) = \psi_1(z)\, H(l - z) + \psi_1(L - z)\, H(z - l).$$

Mode 2

$$\psi_2(z) = \cosh(12.520493156z) - 1.003829\sinh(12.520493156z) + \cos(12.520493156z) + 87.184965\sin(12.520493156z).$$

Hence

$$W_2(z) = \psi_2(z)\, H(l - z) - \psi_2(L - z)\, H(z - l).$$

Mode 3

$$\psi_3(z) = \cosh(16.096693800z) - 0.086689\sinh(16.096693800z) + \cos(16.096693800z) + 41.415181\sin(16.096693800z).$$

Hence

$$W_3(z) = \psi_3(z)\, H(l - z) + \psi_3(L - z)\, H(z - l).$$

11. Normalized Mode Shapes

The normalized mode shape is written as

$$\Phi_n(z) = \frac{W_n(z)}{M_n}, \qquad M_n = \max_{0 \le z \le L} |W_n(z)|.$$

Numerically,

$$M_1 = 850.937886, \qquad M_2 = 87.392498, \qquad M_3 = 43.739875.$$

Therefore,

$$\Phi_1(z) = \frac{W_1(z)}{850.937886},$$

$$\Phi_2(z) = \frac{W_2(z)}{87.392498},$$

$$\Phi_3(z) = \frac{W_3(z)}{43.739875}.$$

12. Final Presentation

Summary of eigenvalues, frequencies and constants

Mode 1 (symmetric)

$$\beta_1 = 4.284723969\ m^{-1}, \qquad \omega_1 = 263.710746\ rad/s, \qquad f_1 = 41.970869\ Hz.$$

$$A_1 = 1, \qquad B_1 = -499.863811, \qquad C_1 = 1, \qquad D_1 = 1700.574330.$$

Mode 2 (anti-symmetric)

$$\beta_2 = 12.520493156\ m^{-1}, \qquad \omega_2 = 2251.775031\ rad/s, \qquad f_2 = 358.381127\ Hz.$$

$$A_2 = 1, \qquad B_2 = -1.003829, \qquad C_2 = 1, \qquad D_2 = 87.184965.$$

Mode 3 (symmetric)

$$\beta_3 = 16.096693800\ m^{-1}, \qquad \omega_3 = 3721.821105\ rad/s, \qquad f_3 = 592.346226\ Hz.$$

$$A_3 = 1, \qquad B_3 = -0.086689, \qquad C_3 = 1, \qquad D_3 = 41.415181.$$

13. Final normalized mode-shape equations

$$\Phi_1(z) = \frac{\psi_1(z)\,H(l-z) + \psi_1(L-z)\,H(z-l)}{850.937886},$$

$$\Phi_2(z) = \frac{\psi_2(z)\,H(l-z) - \psi_2(L-z)\,H(z-l)}{87.392498},$$

$$\Phi_3(z) = \frac{\psi_3(z)\,H(l-z) + \psi_3(L-z)\,H(z-l)}{43.739875}.$$

APPENDIX 5. Acceptance Letter

त्रिभुवन विश्वविद्यालय
TRIBHUVAN UNIVERSITY
इञ्जिनियरिङ्ग अध्ययन संस्थान
INSTITUTE OF ENGINEERING
पुल्चोक क्याम्पस
PULCHOWK CAMPUS
Accredited by University Grants Commission (UGC) Nepal 2020
5-521260
5-521611
5-522104
5-522809
पुल्चोक, ललितपुर।
Pulchowk, Lalitpur

Date: May 9, 2026

To Whom It May Concern:

This is to certify that the paper titled "*Dynamic Behavior Analysis of Beam Supported by Springs with Lumped Mass at the Center*" (Submission ID #944), with **Saurab Kumar Yadav** as the first author, was accepted through the peer-review process and has been presented at the 18th IOE Graduate Conference, organized at Pulchowk Campus, Lalitpur, Nepal, from May 7 to 9, 2026.

Please note that inclusion of the accepted manuscript in the conference proceedings is contingent upon timely compliance with any further editorial requirements during the publication process.

Prof. Sangeeta Singh
Convener
18th IOE Graduate Conference

APPENDIX 6. Similarity Report using iThenticate

Saurab Yadav

PUL080MSMDE021.pdf

Tribhuvan University

Document Details

Submission ID
trn:oid:::3117:585877944

Submission Date
May 4, 2026, 7:19 PM GMT+5:45

Download Date
May 4, 2026, 7:22 PM GMT+5:45

File Name
PUL080MSMDE021.pdf

File Size
2.3 MB

50 Pages

10,588 Words

55,958 Characters

iThenticate Page 1 of 54 - Cover Page Submission ID trn:oid:::3117:585877944

4% Overall Similarity

The combined total of all matches, including overlapping sources, for each database

Filtered from the Report

- Bibliography
- Quoted Text
- Cited Text
- Small Matches (less than 8 words)

Match Groups

45 Not Cited or Quoted 4%
Matches with neither in-text citation nor quotation marks

0 Missing Quotations 0%
Matches that are still very similar to source material

0 Missing Citation 0%
Matches that have quotation marks, but no in-text citation

0 Cited and Quoted 0%
Matches with in-text citation present, but no quotation marks

Top Sources

3% Internet sources
3% Publications
0% Submitted works (Student Papers)

Integrity Flags

0 Integrity Flags for Review

No suspicious text manipulations found.

Our system's algorithms look deeply at a document for any inconsistencies that would set it apart from a normal submission. If we notice something strange, we flag it for you to review.

A Flag is not necessarily an indicator of a problem. However, we'd recommend you focus your attention there for further review.

XL

Match Groups

- **45** Not Cited or Quoted 4%
  Matches with neither in-text citation nor quotation marks
- **0** Missing Quotations 0%
  Matches that are still very similar to source material
- **0** Missing Citation 0%
  Matches that have quotation marks, but no in-text citation
- **0** Cited and Quoted 0%
  Matches with in-text citation present, but no quotation marks

Top Sources

3% Internet sources
3% Publications
0% Submitted works (Student Papers)

Top Sources

The sources with the highest number of matches within the submission. Overlapping sources will not be displayed.

1	Internet	
elibrary.tucl.edu.np		<1%
2	Internet	
ruor.uottawa.ca		<1%
3	Publication	
Yuhao Zhao, Jingtao Du. "Dynamic Behavior Analysis of an Axially Loaded Beam S...		<1%
4	Internet	
www.researchgate.net		<1%
5	Internet	
1library.org		<1%
6	Internet	
uwspace.uwaterloo.ca		<1%
7	Publication	
Kendra Van Buren, Mark Mollineaux, Francois Hemez. "Simulating the Dynamics ...		<1%
8	Internet	
oda.oslomet.no		<1%
9	Publication	
Miles Larkin, Yonas Tadesse. "HM-EH-RT: hybrid multimodal energy harvesting fr...		<1%
10	Publication	
Xiao-Dong Yang, Zhen Li, Wei Zhang, Tian-Zhi Yang, CW Lim. "On the gyroscopic a...		<1%

iThenticate Page 3 of 54 - Integrity Overview Submission ID trn:oid:::3117:585877944

11	Internet	
etd.aau.edu.et		<1%
12	Publication	
Xiubing Yu, Guo Yao. "Nonlinear vibration suppression of a beam subjected to co...		<1%
13	Internet	
mdpi-res.com		<1%
14	Internet	
link.springer.com		<1%
15	Publication	
Fei Hu, Qi Hao. "Intelligent Sensor Networks - The Integration of Sensor Network...		<1%
16	Publication	
Phichaya Suwansaya, Pennung Warnitchai. "Simplified Procedure for Rapidly Esti...		<1%
17	Publication	
Zhuang Wang, Ming Hong, Junchen Xu, Hongyu Cui. "Analytical and experimental...		<1%
18	Internet	
es.scribd.com		<1%
19	Publication	
Bhadbhade, V.. "A novel piezoelectrically actuated flexural/torsional vibrating be...		<1%
20	Publication	
Shiyi Mei, Colin Caprani, Daniel Cantero. "Dynamic response of a combined beam ...		<1%
21	Internet	
pure.tue.nl		<1%
22	Internet	
smartech.gatech.edu		<1%